A Sensor Network for Real-Time Measurement of Aerosol Movement and Persistence for Infectious Disease Monitoring in ICUs and ORs

Kaitlyn Glenn

A thesis

submitted in partial fulfillment of the

requirements for the degree of

Master of Science

University of Washington

2022

Committee:

Igor Novosselov

Michelle DiBenedetto

Elena Austin

Program Authorized to Offer Degree:

Department of Mechanical Engineering

University of Washington

Abstract

A Sensor Network for Real-Time Measurement of Aerosol Movement and Persistence for Infectious Disease Monitoring in ICUs and ORs

Kaitlyn Glenn

Chair of the Supervisory Committee:

Igor Novosselov

Department of Mechanical Engineering

Since the COVID-19 pandemic, air quality has become a public concern due to infectious diseases spread by aerosols. A methodology is presented to map the movement and size of particles using a network of low-cost particulate matter (PM) sensors to determine aerosol persistence in operating rooms (ORs) and intensive care units (ICUs). Mimicking aerosol generation by a patient, we nebulized saline solution to create NaCl particles that function as tracers for potentially infectious aerosols. The ORs rapidly returned to the background after the aerosolization, with a minimum of 94 seconds and a maximum of 254 seconds due to the high air exchange rate. The ICUs had more variability. Positive pressure (door closed) and neutral pressure (door open) ICUs took the longest to clear with a maximum of 830 seconds. Negative-pressure rooms returned to background level to background levels of aerosols on average 1.5-2 times faster than positive-pressure and neutral-pressure rooms (~500 sec). In positive and neutral-pressure rooms, the aerosol plume exfiltrates from the room ~1-2 minutes after the start of aerosolization, with up to 7% of total generated

aerosols escaping the ICUs in positive pressure rooms and up to 17% -- in neutral pressure rooms. The outside sensors in negative-pressure ICUs remained at background levels in each experiment.

After the initial spike at the aerosolization source (head of the bed), the rooms become 'well-mixed' after 100sec, i.e., the aerosol concentration becomes uniform. The PM level reduces the exponential decay rate. Negative pressure ICUs consistently had the fastest decay rate, with an average of 1.5-2 x faster than positive or neutral pressure rooms. Statistical K-means analysis of aerosol spatio-temporal distribution was performed; the clustering algorithm suggested that ICU could be divided into three distinct zones of similar aerosol levels. This gave similar results to zoning the room spatially by sorting the room into (i) the zone near the aerosolization source (the head of the bed), (ii) the periphery of the room, and (ii) the antechamber and directly outside the room. The K-means clustering did not work for ORs since some sensors never saw a rise in aerosol, and the room never became well-mixed. Instead, the OR zones were chosen based on the proximity to the aerosol source. In future studies, long-term monitoring can be attempted, and the current study can be used to inform sensor location and grid density in the network. For example, in ICU, a single sensor instead of using a grid of 16-20 sensors to show aerosol decay could be beneficial to simplify and expedite the experimental process. Experiments in ORs with a prolonged aerosolization period (5 minutes) could show more detailed airflow patterns than those done here (only 1 minute). This research was limited by a small data set (5 ORs and 4 ICUs); additional work monitoring more ICUs and ORs would help validate this work and generalize the monitoring approach. This network monitoring approach can also be extended to other medical settings, such as emergency departments, ambulatory clinics, etc.

1 Contents

Acknowledgments

Throughout the writing of this thesis, I have received a great deal of support and assistance.

I would like to express my heartfelt gratitude towards Prof. Igor Novosselov for giving me the opportunity to work on this project and for his valuable insights and persistent mentoring over the course of this research. Your support and feedback brought my work to a higher level.

I would also like to thank Prof. Michelle DiBenedetto and Prof. Elena Austin for serving on my committee and their support in my academic career.

My sincere thanks also extends to all my fellow students and colleagues in the NRG lab for their help through the different stages of this research. Special thanks to Robert Rochlin and Selina Teng for their help with conducting experiments, coding guidance, many meetings and help with writing.

In addition, I would also like to thank Stephen Scharkov and Rose Hilmo for keeping me sane during some very late nights coding or struggling through data analysis, and their overall excellence as people and friends.

Finally, I would like to thank my friends who supported me (which are too numerous to list here) and especially my family for supporting me all through my school career and dealing with me and my crazy schedule and many projects. Also, thanks to my bunnies Scout and Finch for keeping me constantly vigilant.

2 Chapter 1: Introduction

2.1 Motivation

Since early 2020, exposure to the SARS-CoV-2 virus and its variants has been a significant concern for patients and hospital staff. Like influenza virus and other respiratory diseases, SARS-CoV-2 be spread by inhalation of aerosols containing viable virions. [1, 2]. Hospital environments, such as ORs, ICUs, EDs, etc., are particularly susceptible to the spread of infection, and the aerosol monitoring approaches can aid in combatting the spread of airborne diseases. For example, surfaces and air samples from an ICU with a ready-to-discharge patient previously diagnosed with Covid-19 showed that while all surface samples tested negative, air samples still tested positive, implying that SARS-CoV-2 shed and persisted as aerosol days after a patient tests negative. [3] There have been some efforts to model and measure aerosol movements within hospital environments; [4] however, a systematic approach to characterize the fate of aerosols released in the hospital environment has not been reported. The current practice in controlling the spread of infectious aerosols in ICUs utilizes negative pressure rooms. It has been suggested that aerosols may persist in negative pressure ICUs for 20-30 minutes, and healthcare providers working in the patient room should wear fitted respirator masks and other personal protective equipment (PPE).[2, 5] Without proper characterization, these recommendations remain speculative and may not apply to all ICUs and other medical settings. The data-driven approach can be used to develop more targeted aerosol mitigation strategies to optimize HVAC systems to monitor and minimize the spread of infectious aerosols in medical facilities.

2.2 Background

Recent advancements in low-cost particulate matter (PM) sensors led to their extensive use in various applications, such as air quality (AQ) in indoor environments [6, 7] and outdoor [8, 9],

including large-scale deployments [10-12] by academic researchers and citizen scientists. Optical PM sensors rely on elastic light scattering providing size-resolved PM concentrations in the 0.3 – 10.0 μm range. The low-cost sensor measurements may suffer from sensor-to-sensor variability due to a lack of quality control and differences between individual components.[13, 14] The scattering light intensity depends on particle size, morphology, complex index of refraction (CRI), and sensor geometry. [15] CRI sensitivity can be addressed by optimizing the design to measure scattered light at multiple angles simultaneously or by employing dual-wavelength techniques. [16] However, these solutions are complex and involve expensive components that are not suitable for compact, low-cost devices.[6] As low-cost sensors find applications in pollution monitoring; various studies have evaluated the performance of low-cost PM sensors in laboratory and field settings.[13, 17, 18] These reports show that low-cost sensors yield usable data when calibrated against research-grade reference instruments.[11, 19, 20]

The sensor networks have the potential to provide high spatial and temporal resolution, identifying pollution sources and hotspots, which in turn can lead to the development of intervention strategies for exposure assessment and intervention strategies for susceptible individuals. [21] Recently, low-cost air quality sensors have been used in air quality studies, given their ability to capture high-resolution spatiotemporal data.[22] Data can be fitted to a regression model when analyzing large data sets from such networks. Still, for a large number of sensors and sequentially collected data, conventional techniques may not suffice. Problems with larger dimensions require sequential (or recursive) estimation approaches.[23] An essential factor in the data analysis to simplify or condense the data is to aggregate data from sensors providing that the specifics of the data (such as the locations of the sensor nodes) are not left out.[24]

There is no universal technique for a distributed sensor network data analysis process. However, the k-means clustering algorithm has been used in several wireless sensor networks and has been reported to have many benefits.[25, 26] The k-means algorithm is useful for clustering sensor networks into groups, and it is more efficient to be used in distributed clustering (the method used in this paper) rather than centralized clustering. Distributed clustering methods allow every node to participate in making clustering decisions instead of choosing a 'head' node for each cluster. Clustering algorithms are useful in pattern recognition, artificial intelligence, and statistical analyses. [26]

Several recent editorials are now asking for a new review of airborne transmission indoors and improved guidelines and standards for indoor air handling. [27] For example, Morawska et al. has called for a reevaluation of current air handling standards.[28] Both the National Institute for Occupational Safety and Health (NIOSH) and the Occupational Safety and Health Administration (OSHA) are reviewing and developing standards for workplace environments, including health care facilities.[29]

In summary, numerous studies demonstrated the need for characterization aerosol persistence in indoor settings. There is a lack of space - and time-resolved data on the persistence of aerosols in clinical environments. The few studies that have been reported require cumbersome equipment and are qualitative. For the first time, this paper provides a methodology for obtaining real-time data on the persistence of aerosols in ORs and ICUs using a low-cost sensor network. The data from multiple experiments in four ICU rooms was reduced using the K-means analysis yielding zonal models describing aerosol fate in clinical environments, including aerosol generation and dispersion stages. The zonal models were used to characterize aerosol fate in the OR and ICU under different operating conditions and evaluate the difference between positive,

neutral, and negative pressure rooms in terms of aerosol decay rates, distribution patterns, and aerosol exfiltration.

3 Chapter 2: Experimental Design and Methodology

3.1 Low-cost Particulate Matter Monitor

Time and space-resolved 3D aerosol monitoring require compact devices with accurate particle sizing and fast sampling rate.[30] This study utilized custom PM monitors that incorporate PM sensors, humidity and temperature sensors, Wi-Fi, and cellular LTE chips for data transfer.[31] The data can be transmitted in real-time to the database using a Wi-Fi or cellular connection; the secure digital (SD) card is used for onboard data backup. The data acquisition rate was set to 10 seconds. Each unit incorporates Plantower PMS A003 (Plantower, Beijing Ereach Technology Co., Ltd, China). A sensor's photodiode positioned normal to the excitation beam measures the light scattered by the particles in the optical volume. The scattering light intensity is then converted to a voltage signal to estimate PM number density and mass concentration. The PMS provides particle counts in six size bins in the optical diameter range of 0.3-10 μm range and mass concentration ($\mu g/m^3$) for PM1, PM2.5, and PM10. In the analysis, we report total particle concentration, i.e., all particles with an optical diameter (d_p) > 0.3 μm. This size fraction can stay suspended in air due to their low settling velocities and are a suitable surrogate for long-lived aerosols that may contain SARS-CoV-2 or other infectious agents. [32] Here, original equipment manufacturer (OEM) calibration is used, as relative measurements are sufficient to construct a zonal map of the ICU environment.[19]

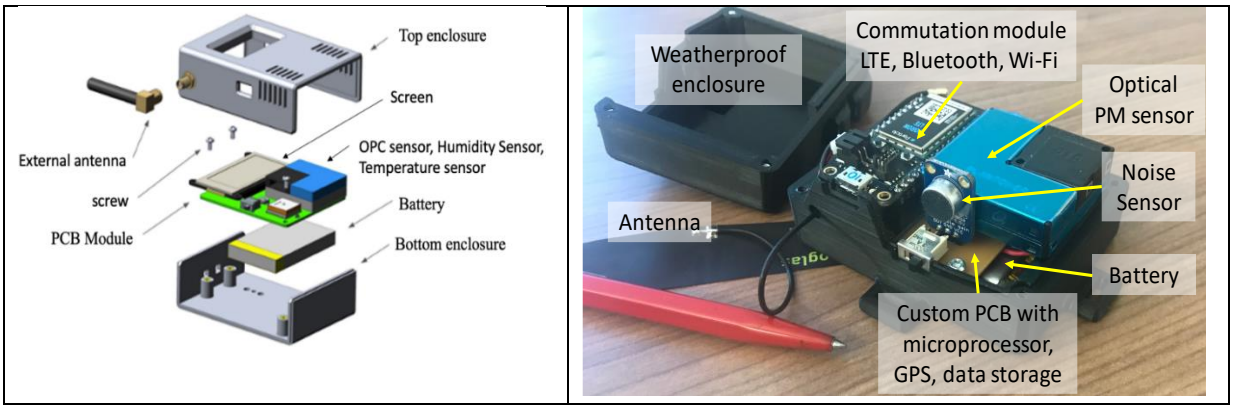

Figure 1: Left: Exploded view of the PM monitor used for the study consisting of PCB board, LiPo battery, and display. The electronics are assembled in an ABS plastic enclosure, with dimensions of (H) 100mm x (W) 60mm x (D) 25mm and weight 120g. Right: IoT-enabled Sensors.

3.2 Experimental Procedure

In a typical experiment, NaCl particles were generated at the location of the patient's head, the aerosol concentration was monitored in real-time until the PM concentration returned to the background level. Particles were generated for 60 sec by nebulizing 1% NaCl solution using the MADA Up-Mist™ Medication nebulizer (MADA Products, Carlstadt, NJ, USA), generating particles in 10nm - 2 µm size range.[33] Once aerosolized, particle behavior is governed by aerodynamic properties, and the chemical composition does not affect their persistence in the environment. The 60-second aerosolization was sufficient to produce enough particles for plume tracking but not enough to saturate the sensors and was below detection to trip the smoke detectors. A short nebulization time is also beneficial as a longer nebulization would result in simultaneous particle generation and evacuation, thereby confounding the analysis. The short nebulization produced an initial spike, following which the particle concentration decayed as the air was exchanged via an HVAC system (through air outlets) or escaped through gaps under the doorway or through the open door. Experiments were terminated when the aerosol concentration in the room reached the background level, < 1 #/cc (total particle concentration).

Particle concentration data with a time-stamp from each sensor were recorded every 10 seconds and saved locally to an SD card. Triplicate measurements were made for each experiment.

4 Chapter 3: Aerosol Persistence in ICUs

4.1 Experimental Setup

This work has been submitted to publication and the preprint is available on MedRxiv.[34] To capture the spatial distribution, we deployed a sensor network consisting of 15-20 PM monitors in a predetermined grid in each ICU and the common areas outside the rooms, see Figure 2. Each monitor in the network is shown as a sphere. The 2-3 hallway sensors are located near the gap of the bottom of the door and another sensor in the hallway about 10 feet from the door. At least one sensor was placed is in the antechamber; if it was present, both negative pressure ICUs had antechambers (as shown in **Error! Reference source not found.**). Aerosol particles are generated at a single location, simulating aerosols' generation (during coughing, sneezing, talking, etc). Similar to the OR study, the location of the sensors in ICU followed a "standard" sensor location grid, expandable or contractible according to room size. This ensures the flexibility and adaptability of our measurement and modeling techniques. The time-resolved PM data from each monitor are aggregated to create a 3D map of aerosol concentration.

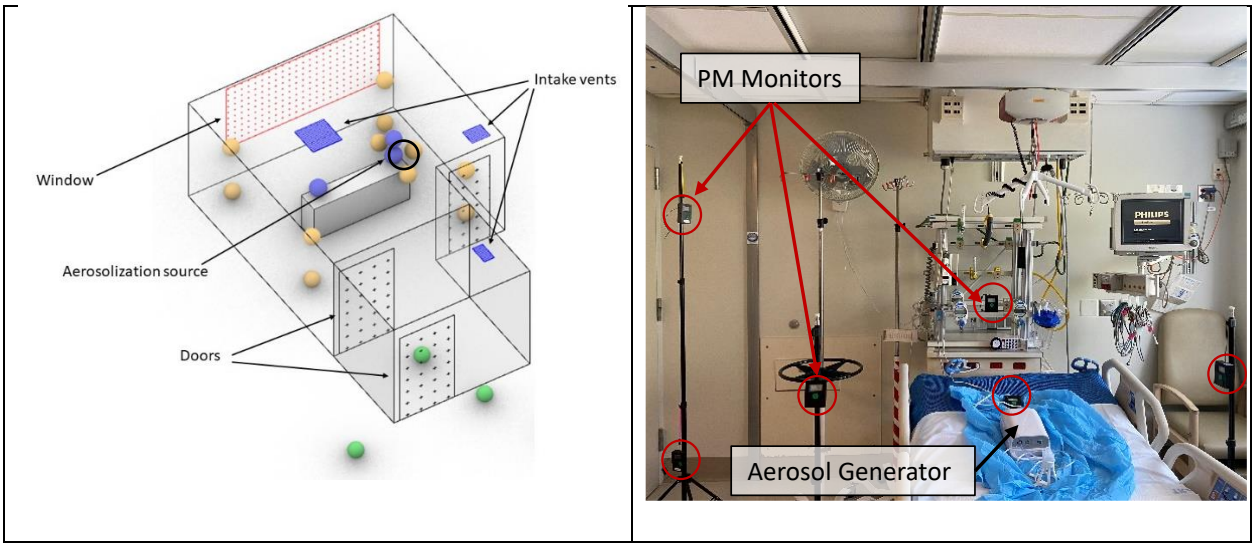

Figure 2: Distributed IoT-enabled low-cost sensor network gathers time and space-resolved aerosol information during aerosol generation, dispersion, and exfiltration stages. The data is transmitted to a cloud server displayed in near real-time. Left: Schematic of typical ICU with sensor locations and locations of

inflow vents, windows, and doors. The black circle represents the aerosolization source. Right: Photograph of the sensor network set up in ICU.

4.2 ICU – Time-resolved Aerosol Distribution

Figure 3 shows a typical 3D resolved aerosol distribution map during the aerosolization and dispersion phases in ICU 1 for positive, neutral, and negative pressure operations. The NaCl particles were generated for 60 sec; the aerosol concentration is monitored in real-time until the level comes to typical background measurements. All experiments show the initial concentration spike during aerosolization at the head of the bed and uniform spreading in the dispersion phase. The analysis of decay rates is presented later in Figures 14-17 and **Error! Reference source not found.**.

PM spike during the aerosolization (t=0-60sec), the aerosol concentration in the room reaches a well-mixed state. At ~100 seconds, the particle plume reaches the outer door of the ICU and escapes the room; the particle concentration outside the ICU door reaches its maximum. The particle plume becomes diluted as it enters the common area. The monitor did not register the particles emitted from the room 20 feet away from the door. The hallway monitors did not register any particles escaping the room.

The concentration spike near the aerosolization source was the lowest with negative pressure – the aerosol was effectively mixed inside the room. This is likely due to the higher air exchange rate (ACR), resulting in greater air velocities (greater turbulence levels) in the room that enhance mixing. The high ACR resulted in a faster return to the baseline level ~500 seconds, compared to ~800 seconds in the positive and neutral pressure cases. Even more importantly, the outside sensors did not register any spikes in aerosol concentration for negative pressure, indicating that the particles generated in the ICU remained in the room. This observation confirmed the efficacy of negative pressure ICU for controlling infectious diseases.

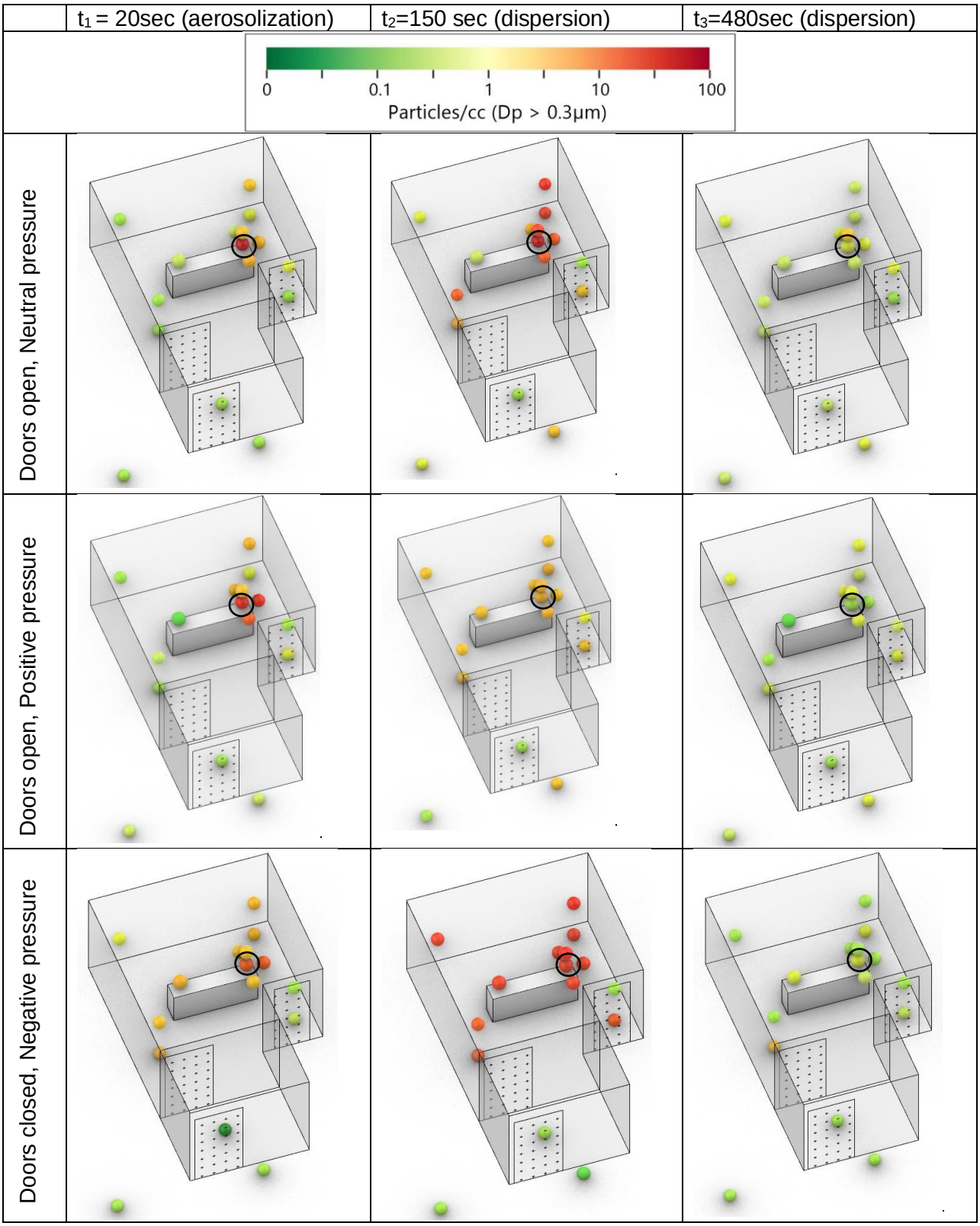

Figure 3: 3D maps from ICU 1 with positive pressure (door closed), neutral pressure (door open), and negative pressure. NaCl particles are nebulized for 60 seconds at the location of the patient's head. Back hallway sensors are located 10-20 feet from the door. The black circle indicates the aerosol source site.

Both positive pressure and neutral pressure conditions showed similar trends. After the initial

In some applications, 3D data visualization can be challenging or not informative. For example, in the large indoor area monitoring, the vertical scale is much smaller than the horizontal; thus, the vertical information can be averaged, or sensors can be deployed on a single level. 2D mapping aggregates the time-resolved sensor data. Figure 4 shows the top-down 2D maps room under positive, neutral, and negative pressure conditions. To generate these images, the room is approximated as a 5x5 2D grid, each grid point with one or more sensors is marked by a number for clarity, if two or more sensors were present at any x/y location (sensors stacked vertically), their data at each time-stamp were averaged. The data for three independent experiments for each time-stamp were averaged. The PM concentration data are then plotted as a spatial heatmap; a linear interpolation is used to approximate the PM concentrations between the sensors. As with the raw sensor data shown in **Error! Reference source not found.Error! Reference source not found.**, the positive and neutral configurations show the initial PM spike at the nebulization source and significant mixing and plum propagation to the antechamber at~100 seconds. At 300 seconds, the entire room and the antechamber are do not have any significant gradient in the PM concentration. In the negative pressure configuration, the aerosol is moving away from the door as the PM level is diluted by the fresh air coming from the hallway. The PM concentrations in antechamber (#10) and the zone adjacent to the ICU door (#8) are at near-background levels for the entire experiment. The data for t=700 sec were not taken since the negative pressure ICU returns to the background before that. Note that the experiments were stopped when the aerosol concentration reached the typical background level of 1 #/cc (or 100 #/0.l L as reported by the low-cost PMS sensor).

ICU Room 1 Neutral Pressure

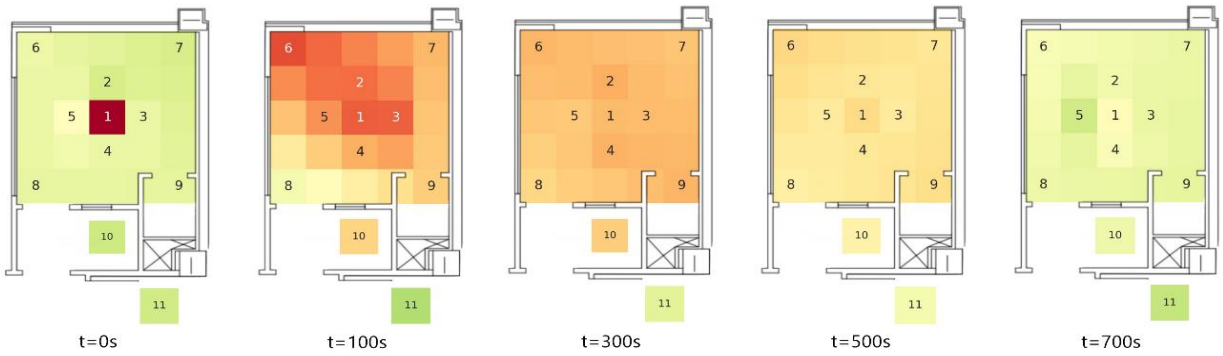

ICU Room 1 Positive Pressure

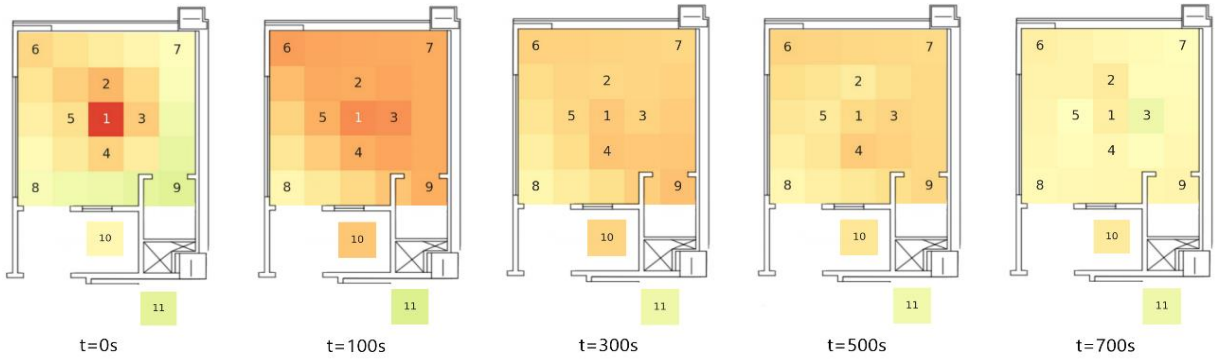

ICU Room 1 Negative Pressure

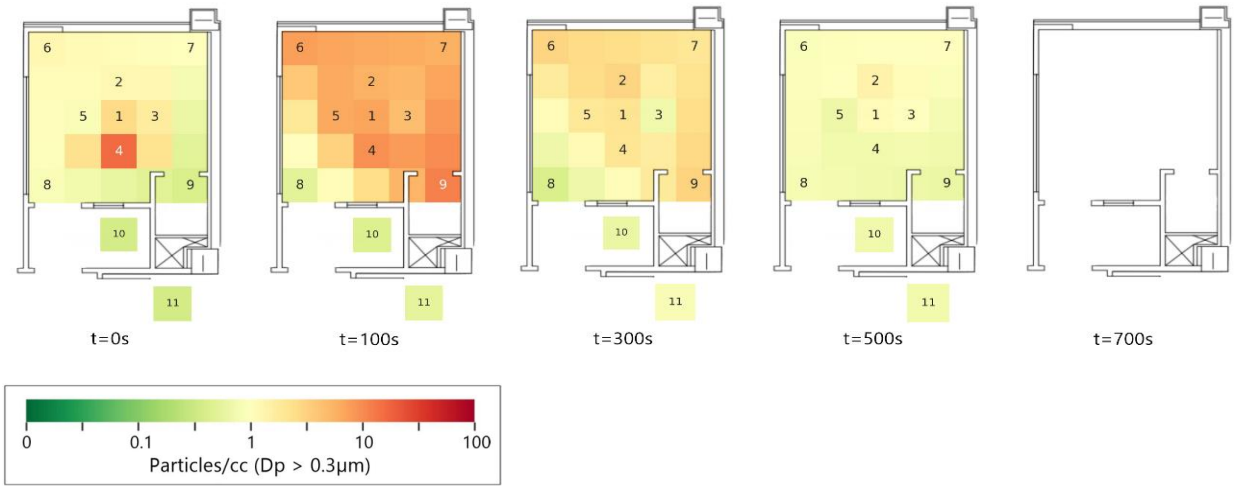

Figure 4: 2D heat maps of ICU room 1 averaged across three experiments for each case of (top) Neutral pressure, (middle) Positive pressure, (bottom) Negative pressure.

4.3 Zonal Analysis

Based on the spatio-temporal trends, the environment can be split into zones where the aerosol concentrations and persistent trends are similar. While these zones could be assigned based on physical location, the data-driven approach could provide insight into aerosol behavior and persistence without *a priori* assumptions and account for PM sources, sinks, and airflow patterns. The results of K-means clustering for ICU 1 are shown in **Error! Reference source not found.**0-13. Similar to the 3D mapping analysis, the sensor data from three replicate experiments were averaged, and three scenarios (positive, neutral, and negative pressure) were evaluated independently for each ICU. Zone 1 sensors are shown in blue; these sensors had the largest and the earliest spike in PM concentration. Zone 2 (shown in orange) spiked later, and their PM levels were consistent. Zone 3 sensors (shown in green) either did not spike very high, had a delayed PM spike in aerosol, or did not rise significantly above the background levels. Note that zone assignment is a function of threshold level (variance between the sensors) set by the user, and the zone assignment can vary, depending on these settings. Figure 9 shows that zone assignment was relatively consistent for each ICU; however, the decay time scale and the clear-out rates between different ICUs differed significantly. For example, in ICU 1, the algorithm had a slightly different split between sensors in Zone 1 and Zone 2; however, Zone 3 stayed the same. Thus, for further analysis, a zonal map for each ICU was fixed based on the positive pressure ICU data, and each ICU was analyzed separately.

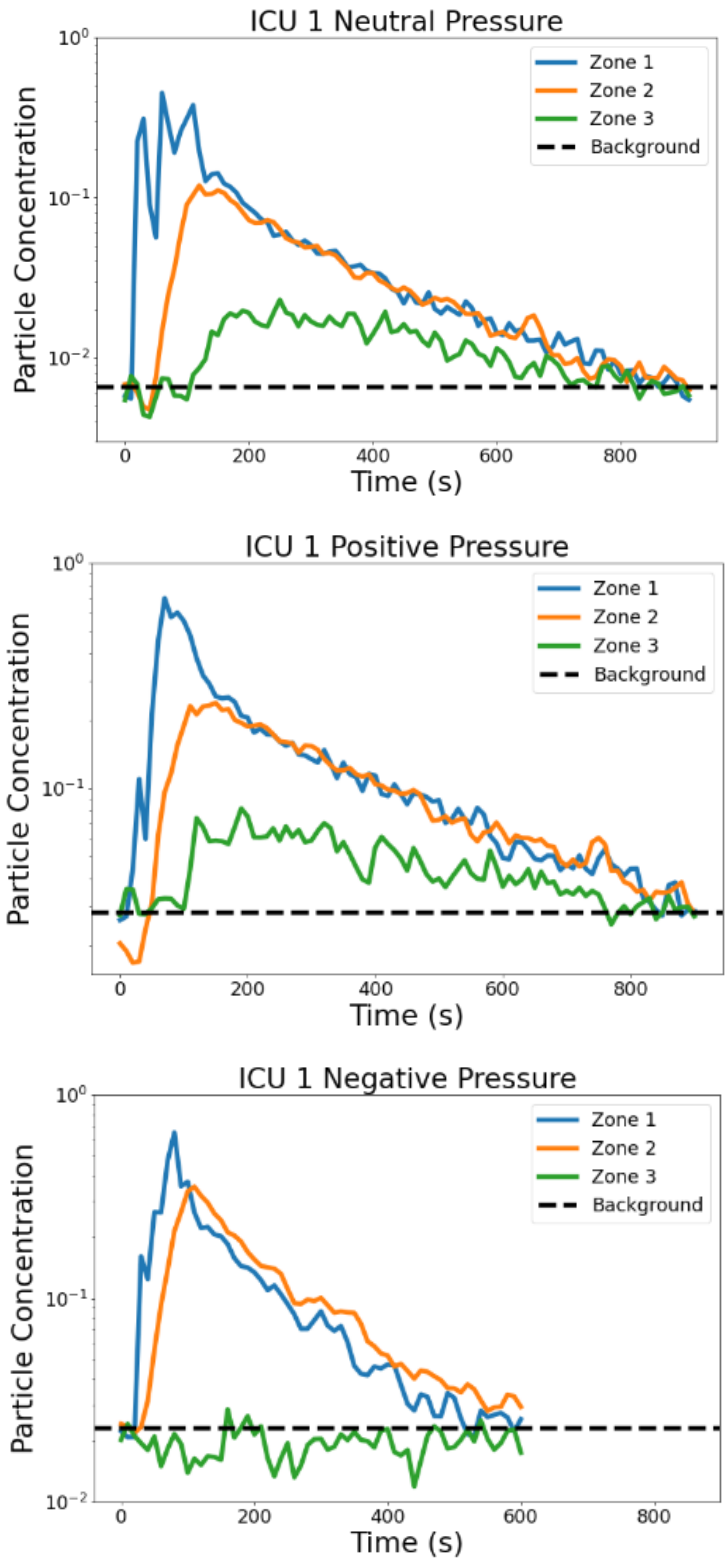

Figure 5: Normalized time data from ICU 1 showing aerosol concentration for each spatial zone compared to background levels.

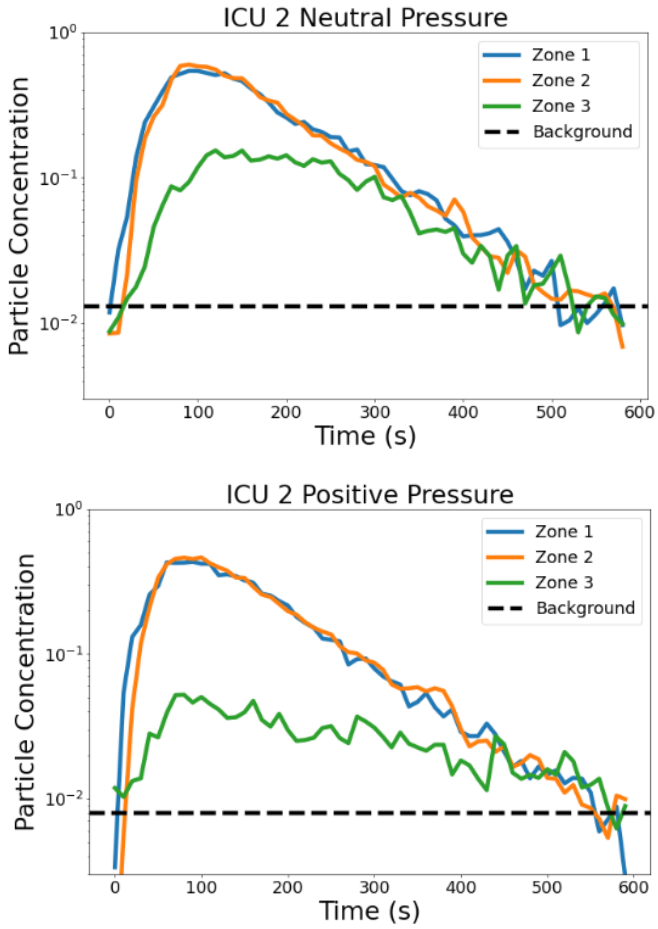

Figure 6: Normalized time data from ICU 2 showing aerosol concentration for each spatial zone compared to background levels.

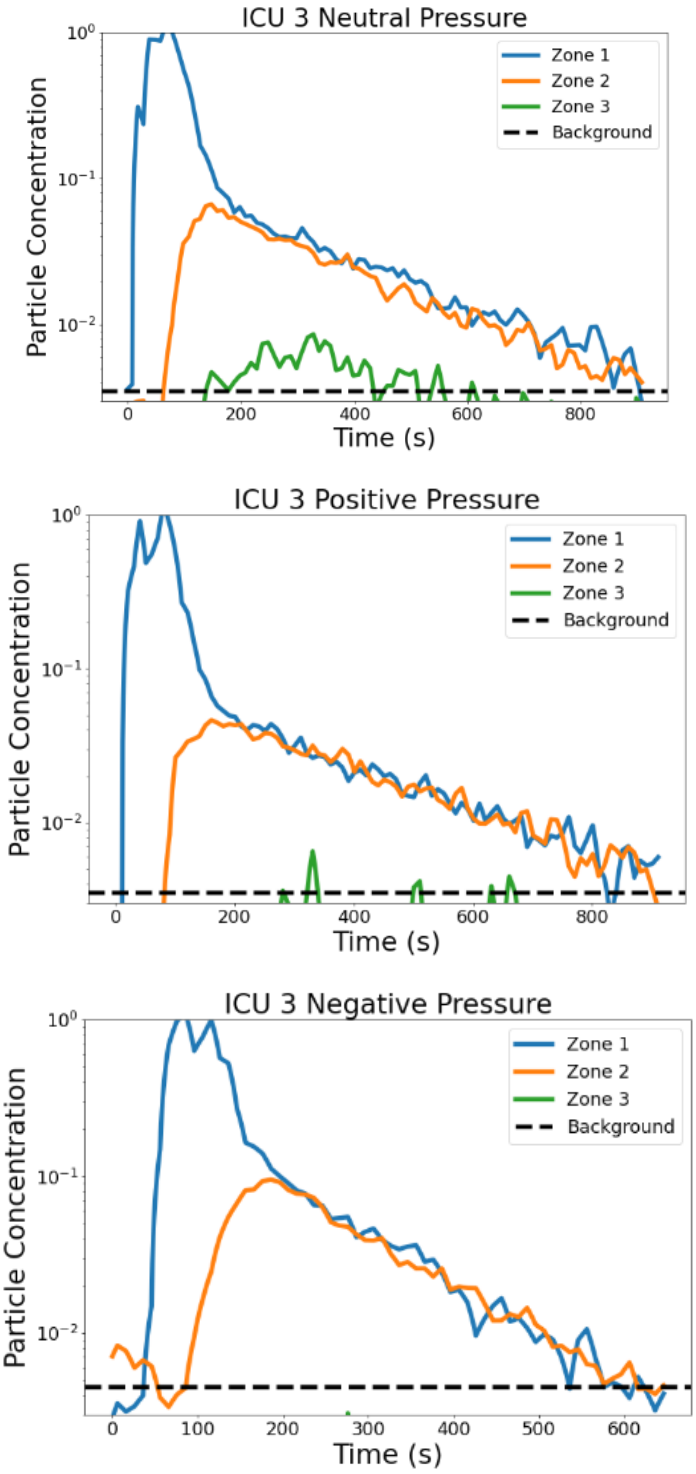

Figure 7: Normalized time data from ICU 3 showing aerosol concentration for each spatial zone compared to background levels.

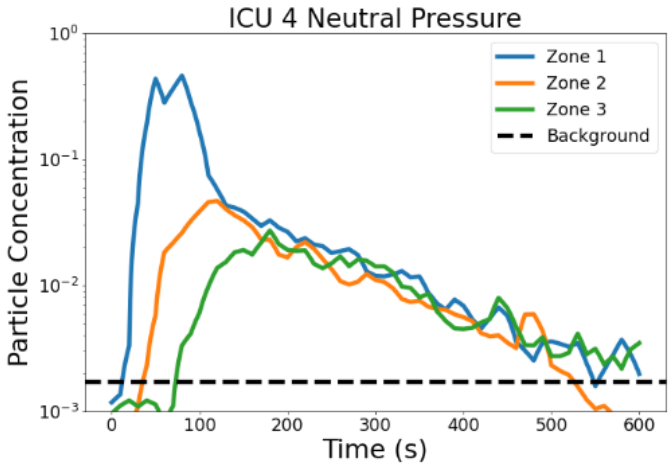

Figure 8: Normalized time data from ICU 4 showing aerosol concentration for each spatial zone compared to background levels.

Triplicate measurements were made for each condition - doors open (neutral pressure), closed (positive pressure), and negative pressure in ICUs. Based on the spatio-temporal information, the sensors were grouped into zones using K-means clustering. [53] The algorithm iteratively finds a globally optimal partition of the data into a specified number of clusters. [54] A clustering algorithm assigns sensors with similar behavior, such as the 'peak' value and when the peak had occurred during the experiment for each sensor. The K-means optimization was implemented using Python code for each experiment and each ICU. The K-means optimization was not used for OR because the rooms never saw a significant change in aerosol since most of the aerosol spike was confined to the head of the bed. Thus, the zones created were not as distinct or helpful in interpreting the data.

Room	Positive Pressure	Neutral Pressure	Negative Pressure
ICU 1	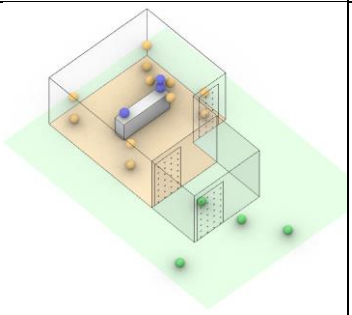	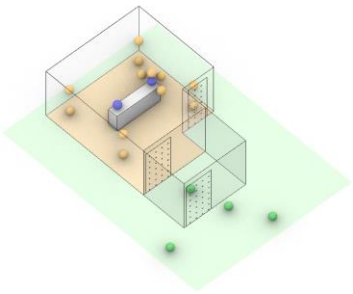	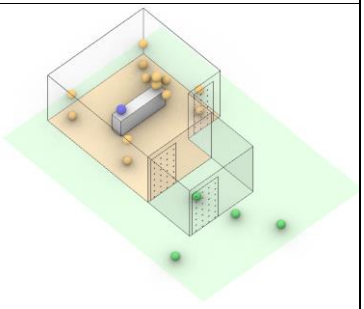
ICU 2	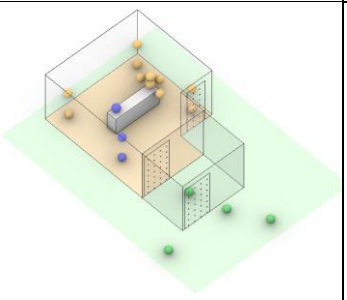	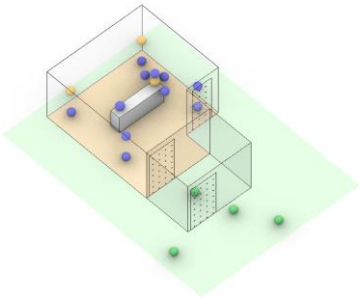	
ICU 3	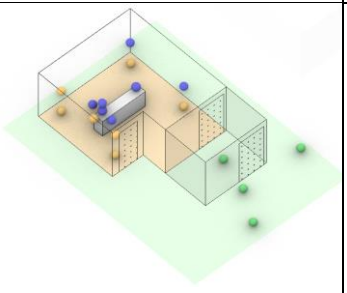	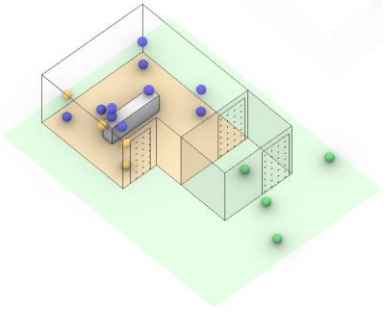	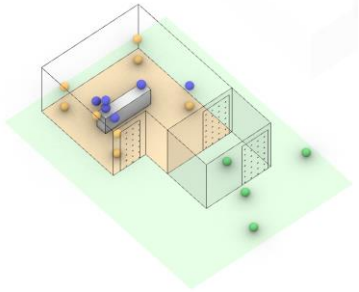
ICU 4		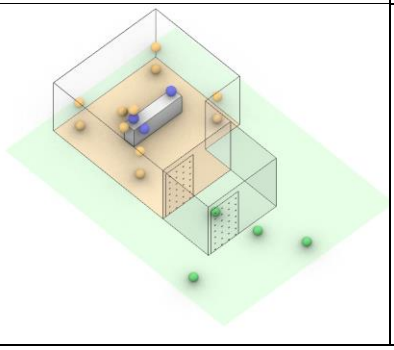	

Figure 9: Automated zones created by the k-means clustering algorithm for each experiment. Blue sensors represent Zone 1, orange sensors represent Zone 2, and green sensors represent Zone 3.

After creating the zones from the K-means analysis, we performed the same data analysis on the ICUs using the new zones. Most of the ICUs showed similar zoning behavior as when we zoned the rooms spatially (1 zone at the bed, 1 zone in room periphery and 1 zone outside).

However, ICU 2 showed Zone 1 as nearly the entire inside of the room, which means that the inside of the room became well-mixed very quickly and stayed at the same levels. We can see from both the spatial and K-means data in Figures 5-8 and 10-13 that Zones 1 and 2 are very similar.

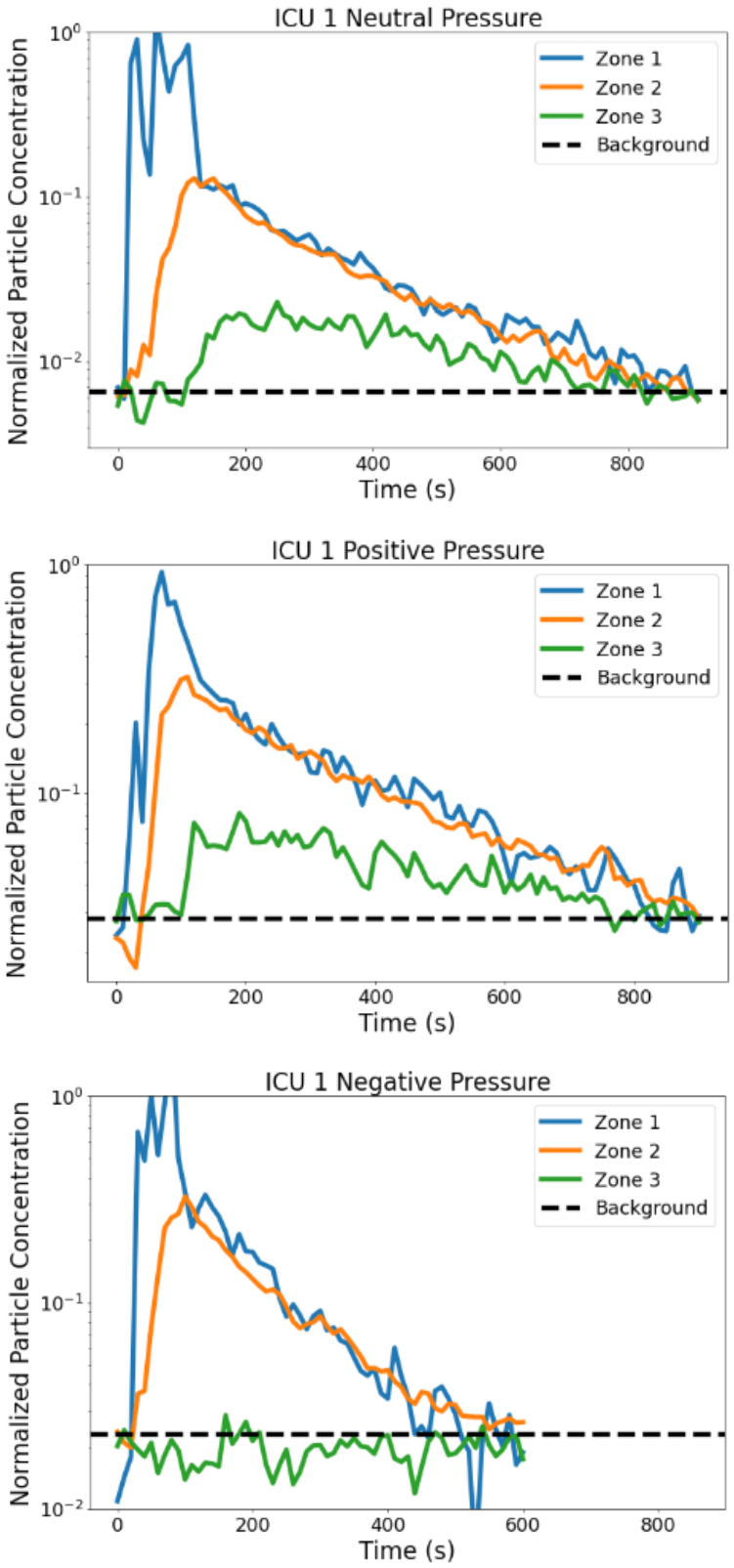

Figure 10: Normalized time data from ICU 1 showing aerosol concentration for each zone compared to background levels.

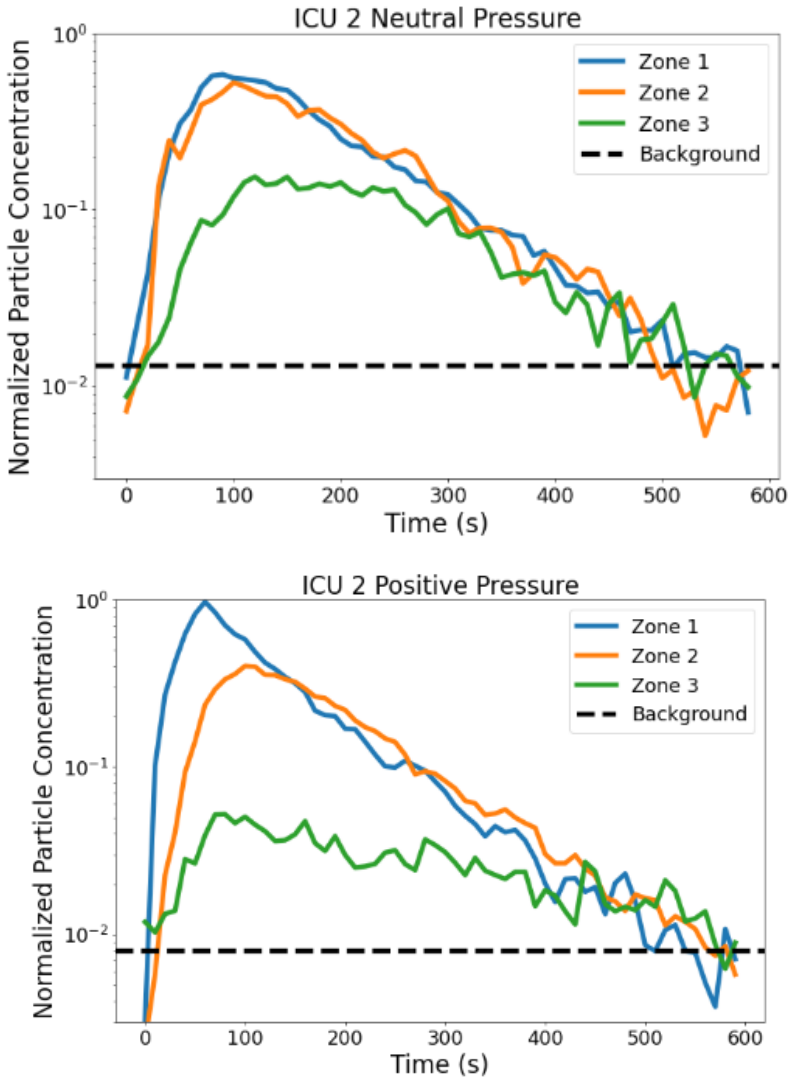

Figure 11: Normalized time data from ICU 2 showing aerosol concentration for each zone compared to background levels.

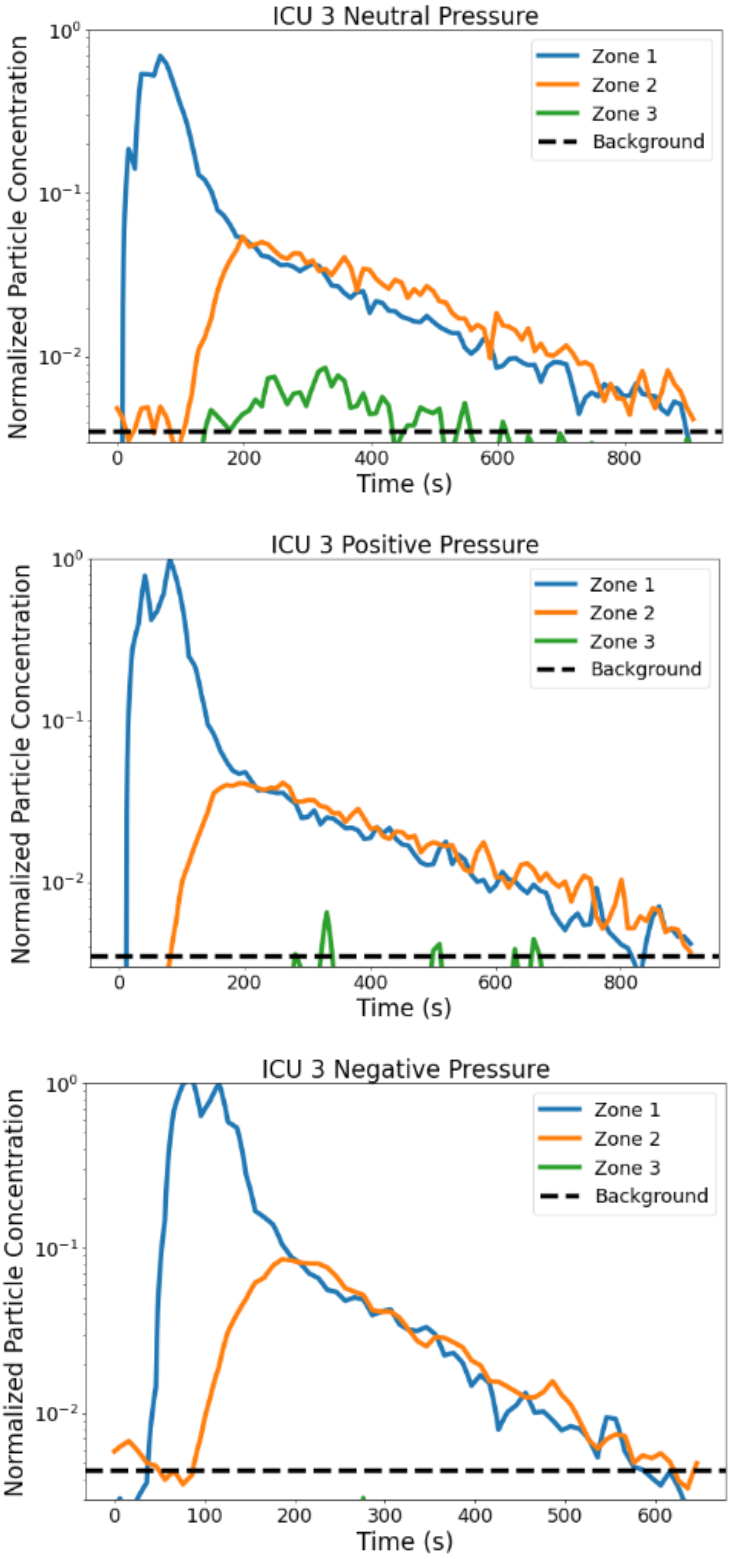

Figure 12: Normalized time data from ICU 1 showing aerosol concentration for each zone compared to background levels.

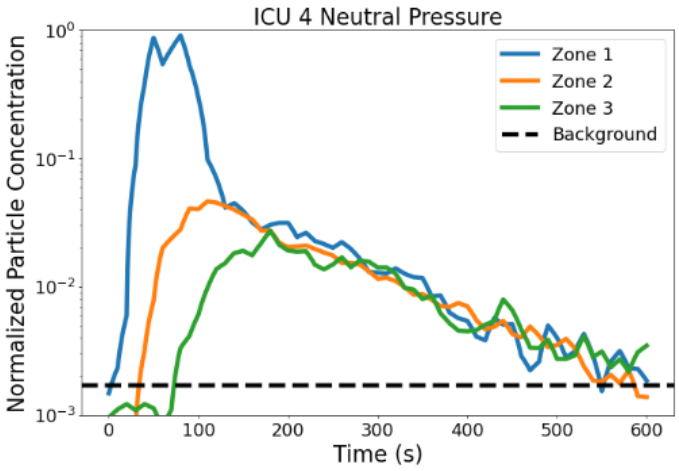

Figure 13: Normalized time data from ICU 4 showing aerosol concentration for each zone compared to background levels.

Figures 10-13 show the time series of the PM concentrations in each zone of each ICU. Since the experimental data had variability in peak concentration (particles/cc), we have normalized the data by dividing all the values by the peak value of that experiment. Consequently, all the decay rates can be plotted on the same scale, and the plots have a maximum value. Overall, the aerosol concentration levels reach the initial background level (1#cc) in positive and neutral pressure ICU at ~ 800 seconds and negative pressure ICU at ~500 seconds. Individual zone behavior can be generalized as follows:

- Zone 1 -- the aerosol concentration spikes immediately with particle generation and then equilibrates to the average room concentration within 30-60 seconds after aerosolization stops.

- Zone 2 -- PM concentration begins to rise within 10-30 seconds and reaches the maximum when the initial peak in Zone 1 is reduced but before the aerosol is diluted by the introduction of filtered air. This indicates that generated aerosol at a point is first dispersed through the room nearly uniformly before it is evacuated by the HVAC system

- Zone 3 -- in the case with positive or neutral pressure, the PM levels are lower as aerosol plume exits the ICU through the gaps around the door or through the open door. For negative pressure, the PM levels are at the background level as the air comes into the room from outside.

Though both internal mixing and removal of PM from the room occur simultaneously, the timescale for these processes in the ICU is different by order of magnitude. The dispersion of the initial spike from Zone 1 to the rest of the room happens over ~30-60 seconds, while the aerosol evacuation (return to the background) takes ~ 500-800 seconds. This separation of time scale suggests that two phases can be identified: (i) aerosol *Dispersion Phase* and (ii) *Evacuation Phase*. The dispersion phase is characterized by the spatial redistribution of the initial PM spike to the room's periphery (from Zone 1 to Zone 2). After the aerosolization is stopped, the PM concentration in Zone 1 rapidly returns to the room's averaged concentration level due to air mixing in the room. During the evacuation phase, the aerosol from a well-mixed room is removed via an HVAC system or exfiltration through the doors and other openings. It is governed by the overall air exchange rate and room condition (i.e., door open or closed, the pressure differential between the room and the outside, etc.). In positive and neutral pressure conditions, the aerosol may particle escape from the room (from Zone 2 to Zone 3); in the negative pressure operation, the air from the adjacent environment infiltrates into the ICU following the pressure differential (from Zone 3 to Zone 2). Additional studies are necessary to determine if the distinction between the phases can be generalized to other settings; the indoor settings, ventilation rates, type of aerosol generation sources, filtration strategies, and other variables are likely to play a role in the duration and overlap these phases. The sensor network approach can be utilized to obtain the necessary temporal and spatial resolution for these analyses.

4.4 ICU Aerosol Decay Rates

The decay rate analysis was performed to generalize the aerosol persistence in the ICUs. During the evacuation phase, the decay rate (DR) was analyzed based on the average of all sensors in the ICU (Zone 1 and Zone 2). The concentration decay appeared linear when plotted on the log-scale against experimental time; however, the decay slopes are different between the ICUs and the operational scenarios. Thus, decay rates were fitted to expression in the form

$$DR = A \exp(bt),$$

where A is a pre-exponential constant dependent on the PM levels of the initial spike, b is the decay constant, and t is the experimental time. The fits for ICU 1 under positive, neutral, and negative pressure are shown in Figure 14 and Table 1.

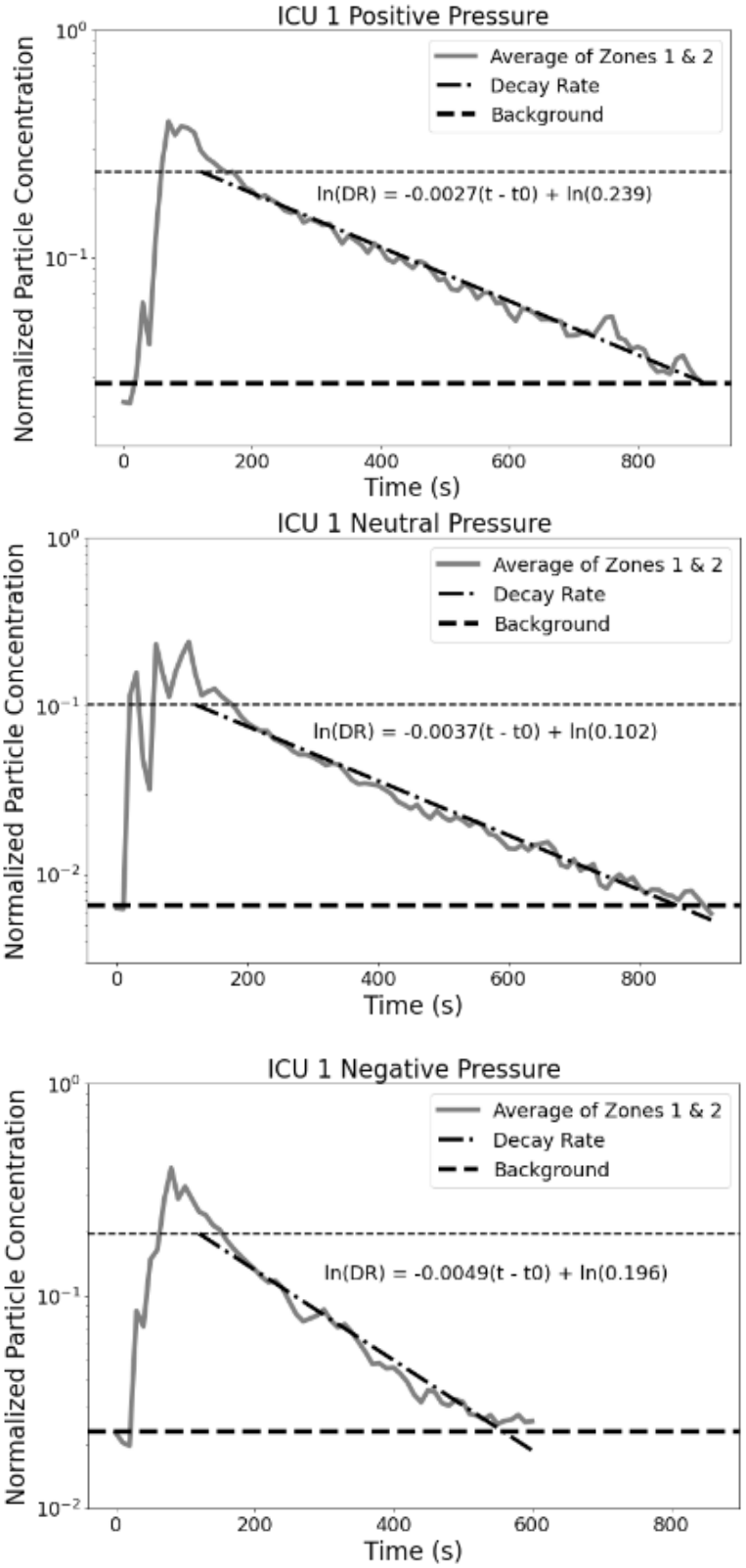

Figure 14: Average time data from ICU 1 showing indoor aerosol concentration and decay rate compared to background levels.

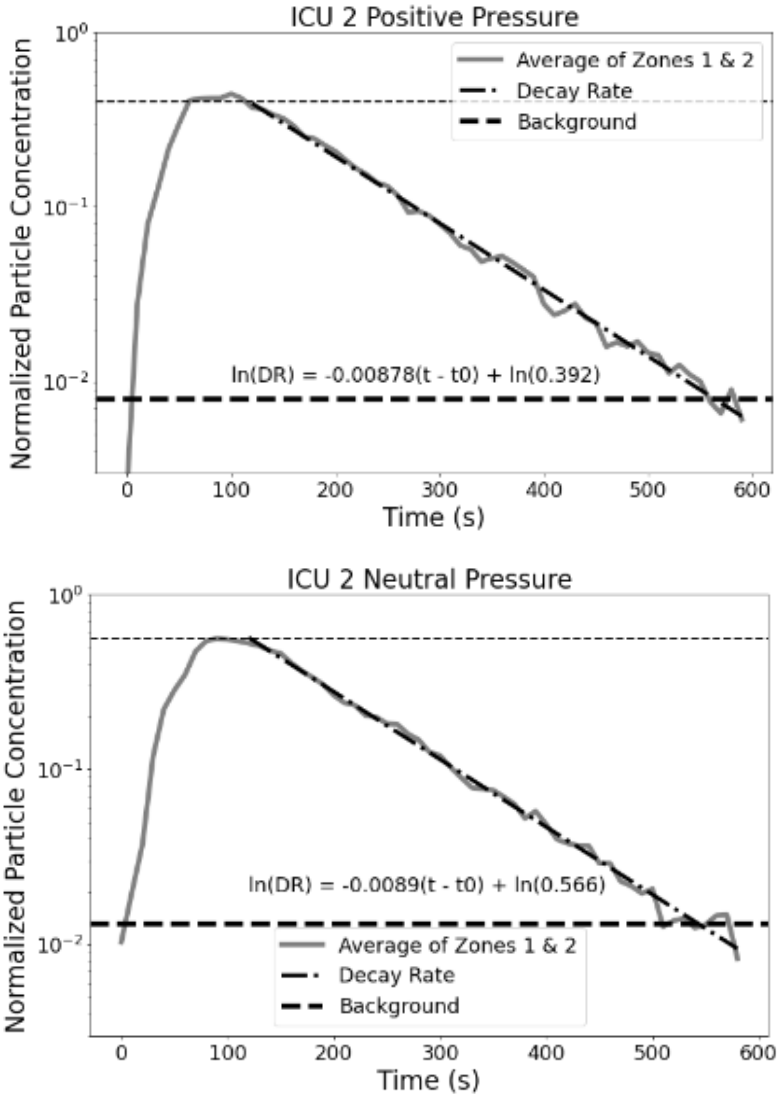

Figure 15: Average time data from ICU 2 showing indoor aerosol concentration and decay rate compared to background levels.

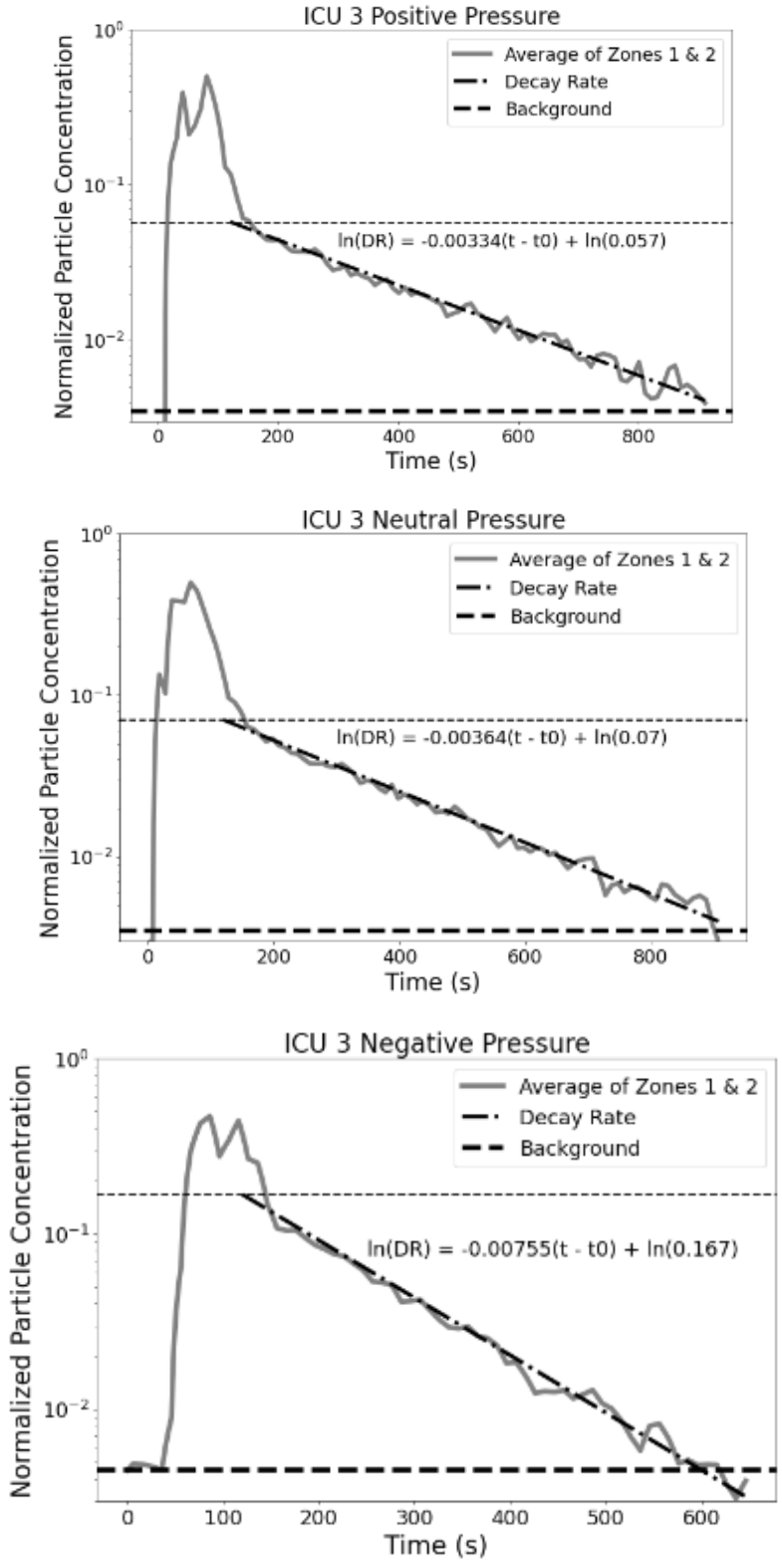

Figure 16: Average time data from ICU 3 showing indoor aerosol concentration and decay rate compared to background levels.

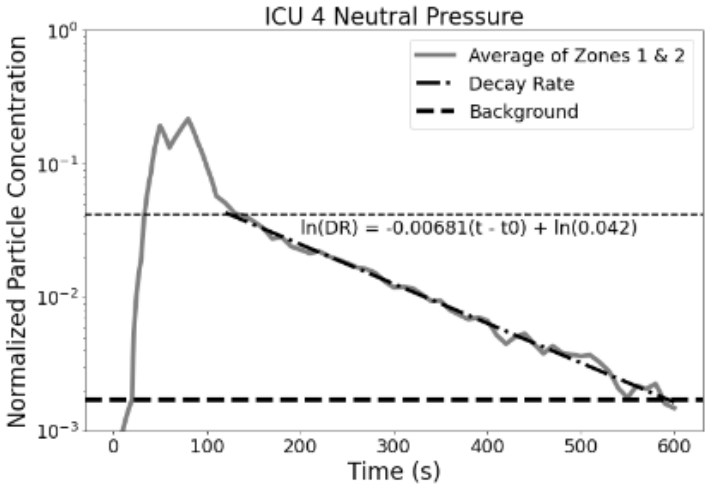

Figure 17: Average time data from ICU 4 showing indoor aerosol concentration and decay rate compared to background levels.

The coefficient (A) of the aerosol spike just depends on where the decay rate line would cross the y-axis and does not seem to follow a specific pattern across experiments but clearly follows a trend within each ICU. The decay rates exponent (b) depends on the specific ICU. In the given ICU, the positive pressure and neutral pressure operation have similar exponents and clear out times as the experimental procedures and the initial aerosol spike were similar in magnitude between the experiments. The decay rates depend on the sensors inside the room and do not include the sensors in Zone 3. ICU 1 clears its PM concentration to background levels nearly twice as fast as the other two configurations in the negative pressure configuration.

In all cases that have negative pressure capabilities, the negative pressure conditions consistently show the fastest decay rates. For the rooms with positive and negative pressure capabilities (ICU1 and ICU3), negative pressure decays on average 1.7x faster than neutral and positive pressure rooms. In each ICU, the neutral pressure configurations always have the slowest decay rates, which means it takes longer to clear out the room, closely followed by the positive pressure configurations. The negative pressure configurations have the fastest decay rates and the fastest

time to clear. Some of the configurations with a slower decay rate have a faster time to clear, but that is because the initial aerosol spike is higher.

Table 1: Decay rate and exfiltration analysis, with the first column as the number of seconds it takes for the room to return to background levels and the second column as the decay rate when all sensors converge to approximately the same decay rate 60 seconds after the end of aerosolization.

ICU	Neutral Pressure		Positive Pressure		Negative Pressure	
	Time to Clear (sec)	Decay Rate (DR)	Time to Clear (sec)	Decay Rate (DR)	Time to Clear (sec)	Decay Rate (DR)
ICU 1	821	$0.159\exp(-0.0037t)$	830	$0.332\exp(-0.0027t)$	450	$0.354\exp(-0.0049t)$
ICU 2	502	$1.648\exp(-0.0089t)$	565	$1.125\exp(-0.0088t)$	N/A	N/A
ICU 3	830	$0.109\exp(-0.0036t)$	830	$0.086\exp(-0.0033t)$	530	$0.415\exp(-0.0076t)$
ICU 4	465	$0.097\exp(-0.0068t)$	N/A	N/A	N/A	N/A

Table 2 estimates the fraction of aerosolized microparticles that was evacuated by the HVAC in the ICU vs the fraction exfiltrated from the room to the common areas. This analysis was performed for well-mixed conditions by comparing the data from the inside (Zones 1 and 2) and outside the room (Zone 3). First, the PM concentration recorded by each sensor (#/cc) was corrected to the coverage area (volume) for the location, which is possible due to the evenly distributed sensor grid and well-mixed zonal condition. Then the particle count from each sensor was added to determine the instantaneous particle count in each zone. As the evacuation phase proceeded, the particle count in each zone was integrated throughout the entire experiment, determining the fraction of aerosolized particles that stayed in the room or exfiltrated to the common area. The procedure was repeated for each experiment and averaged between three replicates to determine the confidence intervals. The authors recognize that several uncertainties complicate the analysis, such as uneven sensor distribution and non-uniform PM concentration within the Zones; thus, this analysis provides the trends in the aerosol fate assessment and not exact values.

Some of the scenarios (particularly negative pressure) show a negative percentage of aerosol, which means the level of aerosol fell below background levels. This implies that aerosol was sucked away from this sensor during the experiment. The neutral pressure scenarios consistently had the most leaked aerosol with a maximum of 17.6%, and the negative pressure scenarios did not exhibit any exfiltration.

By analyzing the number of aerosols at each sensor at various time steps, we can find that in the neutral pressure case, between 2.4% and 20.2% of the total aerosol measured went outside the room. In the positive pressure case, between 0% and 5.9% of the total aerosol measured escaped the room and was detected by the outside sensors. In the negative pressure case, the outside sensors did not measure increased PM concentration.

Table 2: Percentage of aerosols that dispersed to each location (inside the room, under the doorway, and at the nursing station) after aerosolization.

ICU	Negative Pressure			Positive Pressure			Neutral Pressure		
	Inside (%)	Doorway (%)	Nurse Station (%)	Inside (%)	Doorway (%)	Nurse Station (%)	Inside (%)	Doorway (%)	Nurse Station (%)
ICU 1	101.8 ± 1.3	-1.2 ± 0.9	-0.5 ± 0.4	97.5 ± 2.7	6.0 ± 0.1	-3.5 ± 2.6	95.1 ± 1.5	5.6 ± 1.8	-0.8 ± 0.5
ICU 2	N/A	N/A	N/A	94.1 ± 1.9	4.3 ± 1.4	1.6 ± 0.6	86.3 ± 4.2	14.2 ± 1.4	0.6 ± 0.3
ICU 3	103.4 ± 0.8	-2.5 ± 0.5	-0.9 ± 0.3	101.3 ± 0.9	-0.3 ± 0.9	-1.0 ± 0.0	97.5 ± 2.0	2.9 ± 1.8	-0.5 ± 0.3
ICU 4	N/A	N/A	N/A	N/A	N/A	N/A	79.8 ± 2.1	18.5 ± 1.3	1.7 ± 1.0

4.5 ICU Results Discussion

Initial experiments performed in 4 ICUs studied aerosols behavior and flow patterns under negative, neutral, and positive pressure. Adjacent areas such as anterooms and hallways were monitored to assess the presence of fugitive aerosols. This data-driven approach characterizes the aerosol persistence in indoor spaces and allows for monitoring HVAC system performance under real-world conditions. The zone immediately outside of the ICU in the neutral and positive

pressure scenarios shows the presence of fugitive aerosols, while the nursing stations outside the ICU (10-20 ft away from the ICU) do not show the spike in the PM levels. In negative pressure ICUs, there were little to no fugitive aerosols found.

Unlike ORs, ICUs had generalizable behavior. They showed that each zone had an initial spike at different times, then reached a well-mixed condition and exfiltrated aerosol at the same rate. When zoning the ICU via K-Means, the data shown gave the same message as when the room was zoned spatially in terms of decay rates and aerosol exfiltration but could also identify dead zones and hotspots of aerosol. We also were able to find that the aerosol decay rate for a negative-pressure ICU was nearly twice as fast as positive or neutral pressure ICUs, and no aerosol escaped in the negative pressure configuration. The neutral and positive pressure configurations both had similar decay rates, but the neutral pressure rooms allowed up to 20% of the aerosol to escape outside the room into the hallway and outside the ICU, whereas the positive pressure room only allowed up to about 5% of aerosols to reach the surrounding areas.

These experiments provide the baseline for modeling the persistence and dispersion of aerosols in both ICUs and non-ICU clinical spaces. In future measurements and analysis, we will optimize sensor number and location and assess and model for adaptability for different physical clinical locations as well as built-in elasticity to the models. Methods of choosing the number of sensors and their placements have been outlined before for complex dynamical systems and could be applied to these sensor networks. Extension of sensor network measurements, data integration, and visualization to other patient care environments would inform the optimization of air handling strategies and minimization of risks from potential airborne infectious agents in additional less well-defined clinical areas.

5 Chapter 4: Aerosol Persistence in Operating Rooms

The location of the sensors in a representative OR, shown in Figure 18, is a "standard" sensor location grid, expandable or contractible according to room size. This ensures the flexibility and adaptability of our measurement and modeling techniques. All of the ORs we measured have inlet vents located above or near the OR table, with three or four outlet vents situated at floor level, usually in the corners. The air inlet is located above or nearly above the bed.

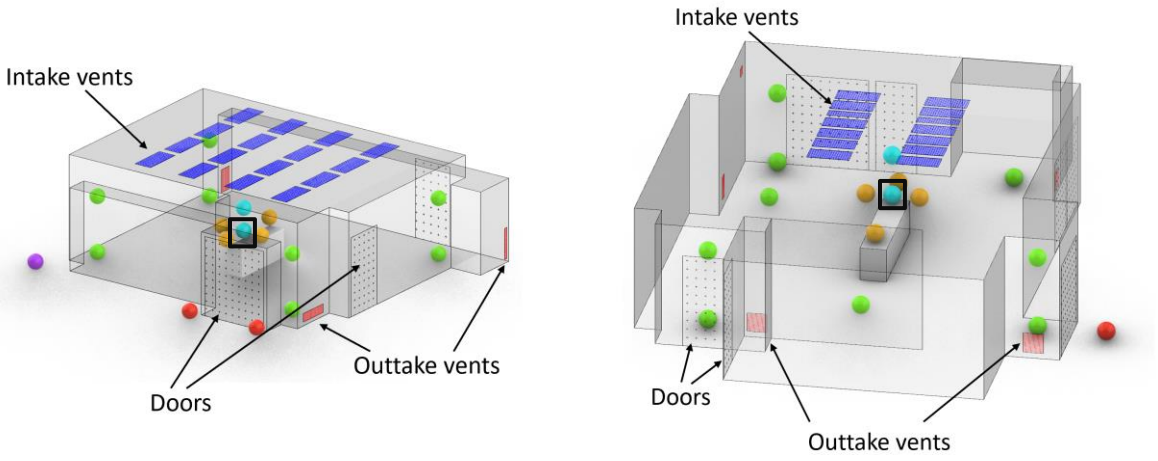

Figure 18: Schematic of typical ORs (Left OR-C, Right OR-D) with sensor locations and location of inflow and outflow vents. The air inlet is located above or nearly above the bed and is shown as blue rectangles; each dot represents a sensor, while red squares represent outlet vent locations. Sensors are located close to the gap at the bottom of the door to capture aerosol plume propagation to the hallway. The background sensor is positioned in the hallway, 10-20 feet from the OR door. Sensors are grouped into zones based on proximity to the aerosol generation source and on similarities in time-resolved particle concentration behavior.

5.1 Initial Harborview Medical Center Experiments

We conducted the first experiments in Harborview Medical Center (HMC, OR-A). These initial experiments evaluated the overall approach and informed the future study, so these initial results vary more than the results from UWMC. However, the data presented in this thesis for completeness. There were no sensors outside the room, and in one of the experiments, we

aerosolized the NaCl particles for 5 minutes instead of 1 minute. Figure 19 shows the time-stamped data from sensor measurements. The sensor locations are shown as small spheres colored by the PM concentration (#/cc).

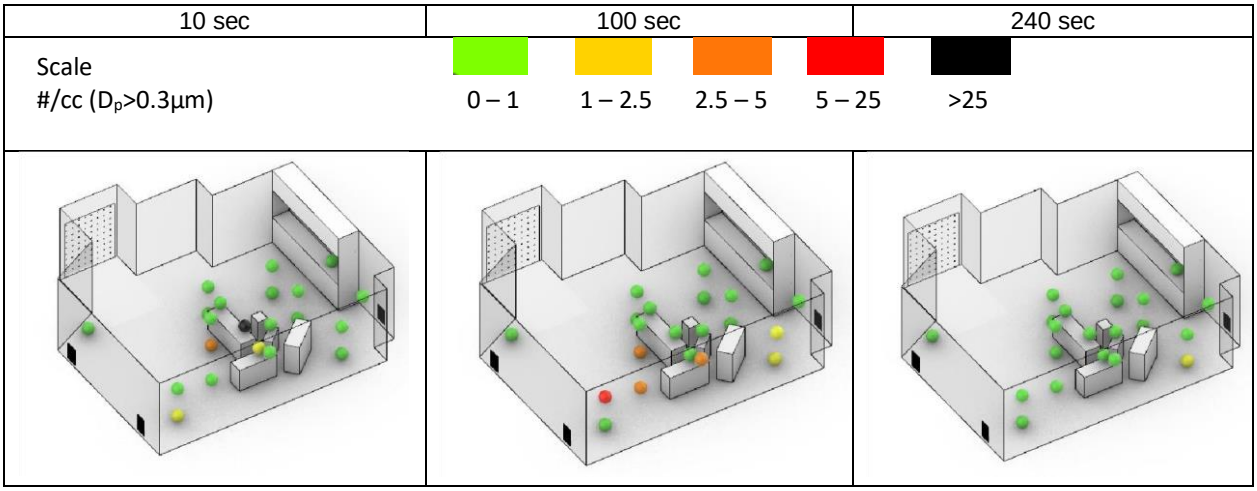

Figure 19: Example 3D map from OR-E. Aerosolization occurred at the head of the bed for 1 minute, and results are shown at 10s, 100s, and 240s.

The time-resolved data is shown in Figure 20 by separating the data into three zones, with Zone 1 consisting of the sensors closest to the aerosolization source, Zone 2 consisting of the sensors around the bed, and Zone 3 consisting of the sensors at the room periphery. The 1-minute aerosolization experiment had a high variation in sensor data, but in the third experiment (with the 5 minute aerosolization period), there was an evident rise and fall time for all the zones.

Figure 20 shows the time evolution of the PM levels in each zone based on the average of three trials for each condition. The left image shows the experiment in which NaCl particles were nebulized for 1 minute, and on the right, the experiment in which NaCl particles were nebulized for 5 minutes. Since some sensors showed significantly higher aerosol levels than others, the data is shown on a $\log_{10}$ scale for comparison purposes. The data are also normalized to the maximum sensor measurement. The dashed line represents the background PM level at the start of the experiment. Both experiments ran until all the sensors reached (or got very close to) background

levels. Since the first experiment had a short nebulization time, the room was not fully saturated with aerosols as it was in the 5-minute nebulization experiment and thus cleared out much faster. The analysis of the decay rates is presented later in the thesis.

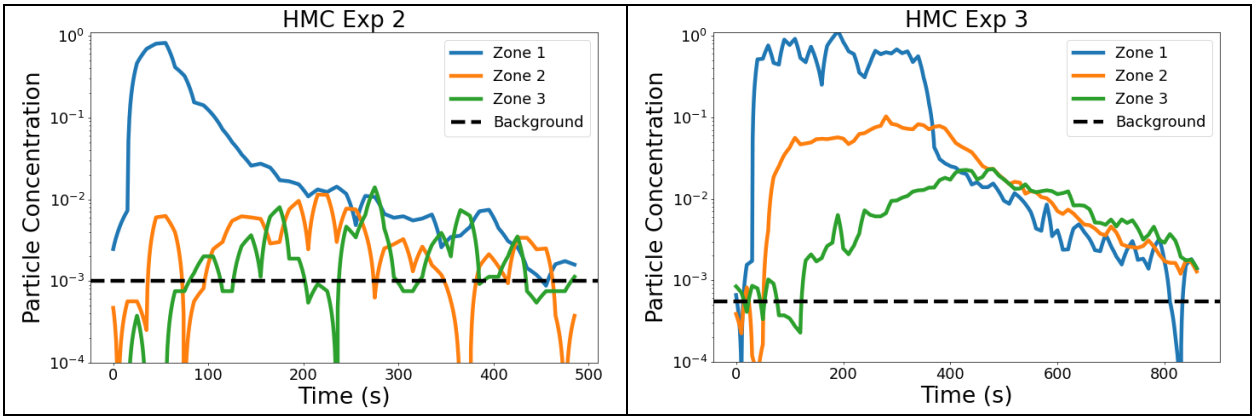

Figure 20: Normalized time data from OR-E showing aerosol concentration for each zone compared to background levels.

The time-resolved data and the 3D maps show that the room cleared out quickly, and the only significant spike in aerosol concentration was detected near the aerosol source. However, when the aerosolization period is set to 5 minutes instead of 1 minute, we clearly distinguish between the three zones. Zone 1 spikes the highest and soonest, then Zone 2 and Zone 3 following soon after. Soon after the aerosolization is stopped, the room becomes 'well-mixed' where all the zones converge to approximately the same aerosol concentration. The PM level decay as the aerosol is evacuated by the HVAC system until the room returns to the background levels.

5.2 UW Medical Center OR Experiments

5.2.1 Study design

Informed by the initial experiments at HMC, the UWMC OR monitoring approach was more systematic. Four OR rooms were studied (ORs B-E). The location of the sensors in a representative OR, shown in Figure , is a "standard" sensor location grid, expandable or contractible according to room size. This ensures the flexibility and adaptability of our

measurement and modeling. All ORs had inlet vents above or near the OR table, with three or four outlet vents situated at floor level, usually in the corners. Airflow velocities for each outlet and the door gap at the bottom of the door were measured using a hot-wire anemometer. Table 1 presents the dimension of the ORs and the flow rates. Additional sensors were placed outside the room to monitor fugitive aerosol escaping the room and background concentration in the facility. Aerosol particles were generated at a single location at the head of the bed.

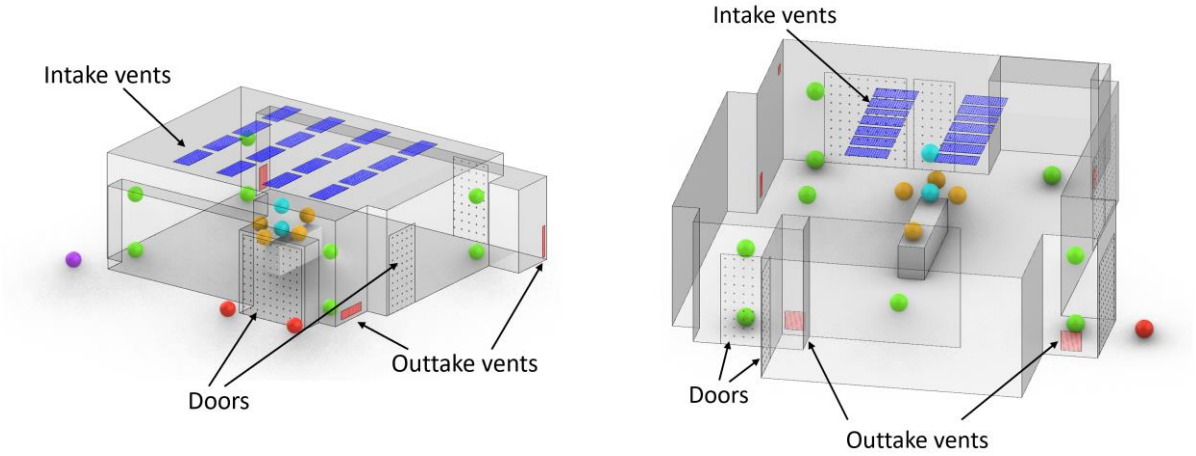

Figure 21: Schematic of typical ORs (Left OR-C, Right OR-D) with sensor locations and locations of inflow and outflow vents. The air inlet is located above or nearly above the bed and is shown as blue rectangles; each dot represents a sensor, while red squares represent outlet vent locations. The hallway sensors are located close to the gap at the bottom of the door to capture aerosol plume propagation to the hallway. The background sensor is positioned in the hallway, 10-20 feet from the OR door.

Table 1. OR room dimensions, and the number, location, dimensions and measured flow rates for intake and exhaust vents

Room	Overall Dimensions		Outlet vents		Doors (Underneath)		Room Air Supply	Room ACH
	Dimensions (m)	Volume (m^3)	Total Area (m^2)	Flow Rate (m^3/s)	Total Area (m^2)	Flow Rate (m^3/s)	Ft^3/minute	Air Exchanges per Hour
OR B	7.3 x 7 x 2.7	143.1	0.44	0.711	0.025	0.106	2310	27.4
OR C	7 x 7.6 x 2.8	151.5	0.47	0.635	0.067	0.284	2700	30.3
OR D	7.8 x 9.4 x 2.8	252.1	0.74	0.974	0.156	0.531	2700	18.2
OR E	7.2 x 7.3 x 2.8	138.5	0.44	0.922	0.081	0.331	2180	26.7

5.2.2 3D mapping of Aerosol Concentration in UWMC ORs

For each experiment, the PM data was first synced to the start of the nebulization (used as the datum). The sensor readings were averaged in 10-second epochs for each sensor; these data were used to create a time-resolved 3D map of aerosol distribution. The data for each experiment are plotted as a 3D map at given time-stamps (Figure 22) and linearly (Figures 23-26).

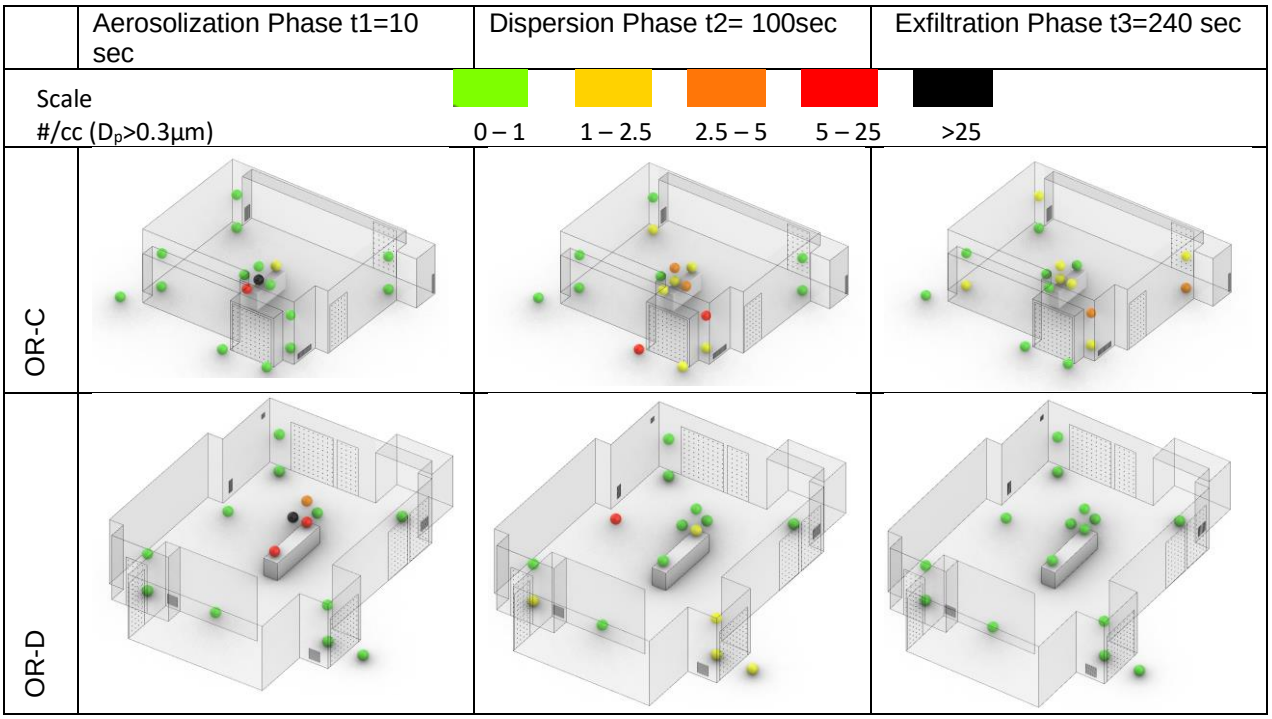

Figure 22: 3D maps of OR-C and OR-D during aerosolization and particle dispersion stages. NaCl particles are aerosolized for 60 secs from a position at the head of the OR table. Sensors are deployed in a predetermined pattern, shown as the points colored according to real-time PM concentration.

Figure 22 shows a typical 3D resolved aerosol distribution map during the aerosolization and dispersion phases in OR-C and OR-D for operations. The NaCl particles were generated for 60 sec; the aerosol concentration is monitored in real-time until the level comes to typical background measurements. All experiments show the initial concentration spike during aerosolization at the head of the bed and non-uniform spreading in the dispersion phase.

5.2.3 Zonal Analysis of Aerosol Decay in OR

The following plots show the results for each OR, based on three replicates. The background level is defined as the average aerosol level before the experiment began, and the data is zoned spatially. Sensors are grouped into zones based on proximity to the aerosol generation source and similarities in time-resolved particle concentration behavior. Zone 1 is directly around or on the head of the bed (source of aerosolization), Zone 2 is the room periphery, and Zone 3 consists of the outdoor sensors.

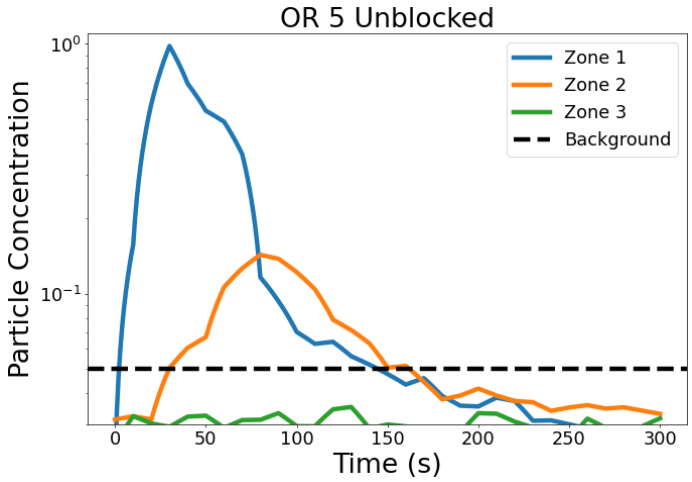

Figure 23: Normalized time data from OR-5 showing aerosol concentration for each zone compared to background levels.

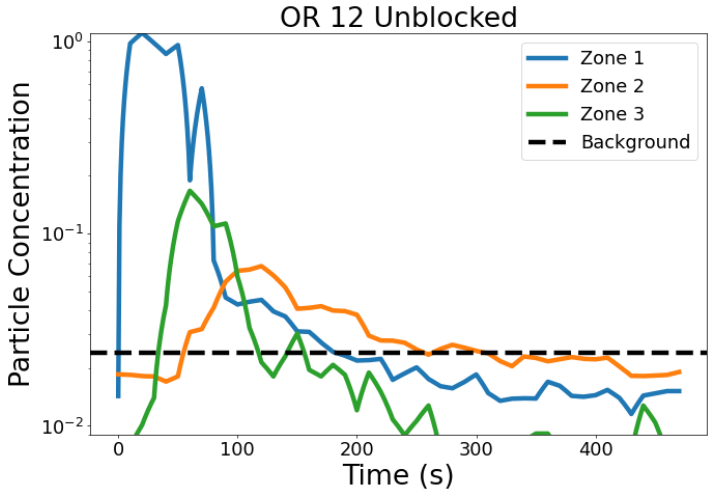

Figure 24: Normalized time data from OR-12 showing aerosol concentration for each zone compared to background levels.

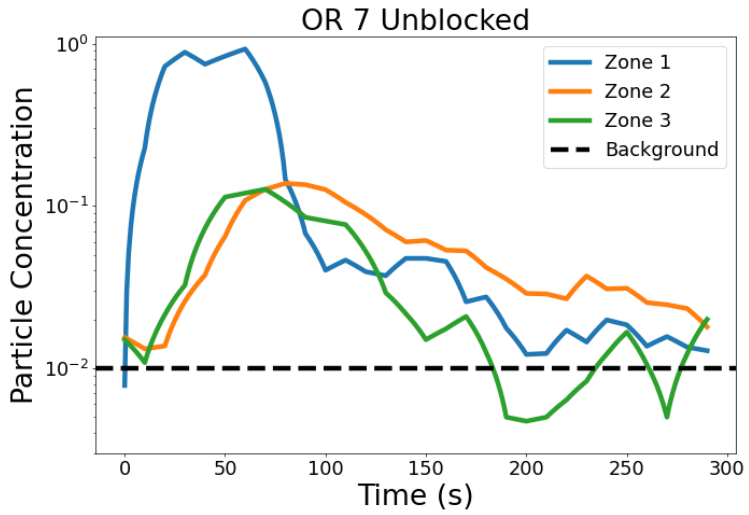

Figure 25: Normalized time data from OR-7 showing aerosol concentration for each zone compared to background levels.

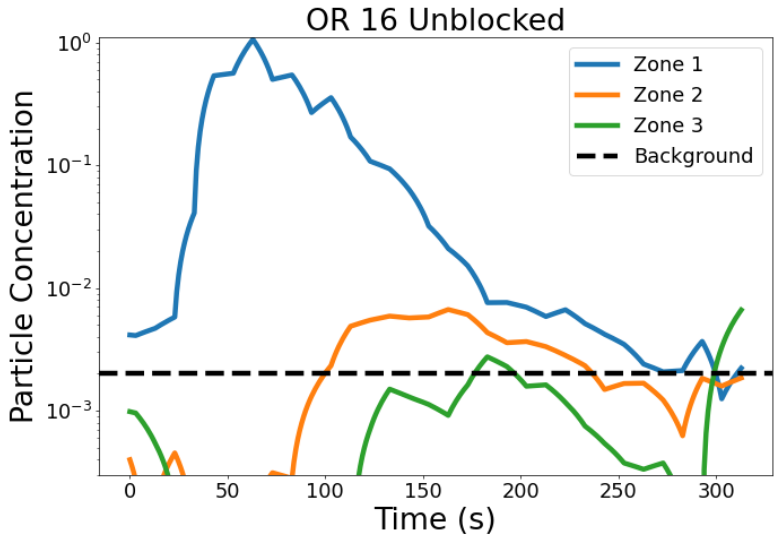

Figure 26: Normalized time data from OR-16 showing aerosol concentration for each zone compared to background levels.

Table 3: Time required for each OR to return to background levels in each experiment.

OR	Time to Clear (seconds)	
	Open	Blocked
OR-A	94	99
OR-B	101	123
OR-C	253	254
OR-D	140	157
OR-E	230	N/A

In each experiment, the aerosol returns to background levels within 1.5 - 4.5 minutes, which is fast for such a big room. Though it is not included in this table, the OR-A experiment in which the aerosolization period is changed to 5 minutes instead of 1 minute causes the time to clear to rise from 30-200 seconds after the end of aerosolization up to 600 seconds after the end of aerosolization. In ORs, future experimentation could be done using a more extended aerosolization period to show airflow patterns, rates, and 'dead zones.'

5.3 Chapter 5: Discussion and Future Work

5.3.1 Indoor Monitoring

Flexible deployment of a low-cost sensor network offers real-time, space-resolved 3D monitoring that is not achievable by traditional methods. Alternative instruments are expensive, bulky, and only provide single-point measurements without real-time monitoring capabilities. Our initial deployment of a 25-sensor network in the UW Harborview Medical Center (HMC) operating room demonstrated the approach's feasibility. We were able to visualize particulate concentration in real-time and quantitatively describe the persistence of fine particles after the aerosol generation events. The team has also evaluated the approach in the recent deployments at Boeing manufacturing facilities and pilot epidemiological studies. However, the time-resolved 3D aerosol measurements in medical facilities have not been presented in the scientific literature outside of our initial experiments.

The data accuracy from low-cost devices, especially in informal networks, is a contentious point in air quality research. The data quality without regular on-site calibration can come under scrutiny, and the on-site calibration can be costly, especially for large deployments [12, 35]. For example, Jiao et al. evaluated a wide variety of low-cost PM sensors; some sensors had a good agreement between identical sensors but moderate agreement with a reference PM2.5 instrument

(e.g., R = 0.65) [9]. Multiple authors reported in-situ calibration and data correction strategies in the network deployment [36]. Kelly et al. reported that in ambient tests, the PMS sensor correlates well with gravimetric methods and not with particle counts [18]. This was confirmed by Huang et al., who showed that OEM calibration for the number density concentration of the same sensor is not inaccurate; however, the calibration for $PM_{2.5}$ compared well over the range of PM concentrations and CRI values.

The sensor network addresses several market sectors, including medical facilities, occupational settings, sports venues, public spaces, government buildings, and the consumer market. Applications in medical facilities operation can be related to optimization of the existing infrastructure through providing periodic consulting services or permanent installation of the fixed sensor networks in areas of interest (OR, ICU, ED). In occupational settings, our approach provides a solution for businesses to improve indoor air quality systems to address worker safety, especially in an environment with high PM loading. For government entities (schools, public spaces, government buildings), the sensor network provides real-time information on indoor air quality during periods of wildfires or other poor air quality events and informs the decisions on building operations. In the consumer markets, we envision sensor sales with a personalized app interface for monitoring household PM levels (room-by-room) and suggesting potential indoor air quality improvement strategies.

Mitigation strategies for potentially infectious aerosols can include using air purifiers to minimize the infection risk of COVID-19 and other infectious aerosols. We will work with Harborview MC, UWMC, and UW School of Dentistry (SoD) personnel to develop evidence-based solutions for the operation of medical facilities and other public spaces. The sensor network will inform the decisions on HVAC operations, operating room scheduling, optimization of air

filtration in ICU, EDs, ambulatory clinics, dental offices, etc. The sensor network operation would include installing the fixed sensor networks in areas of interest and supplying a network service, including data analysis. The proposed personal exposure monitor is a wearable device about the size of a smartphone. The monitor measures the PM level and gaseous pollutant concentrations in real-time. When deployed, stationary and personal exposure monitors can form a crowdsourcing sensor network that will capture the detailed pollution distribution on a neighborhood scale in real-time. The data from the sensor network will be used to generate a hyper-resolution pollution heatmap that susceptible individuals can use to plan their daily activities. The household monitor can inform the residence about the AQ in their household and deploy interventions such as additional filtration units, upgrades to central air handling.

The sensor network measurements, data integration, and visualization to other patient care environments will allow us to optimize air handling and minimize risks from potential airborne infectious agents in additional less well-defined clinical areas. The team is already evaluating how the technology might be deployed in clinical workplaces post-COVID-19. For example, the long-term installation might monitor larger areas to assess data-driven control strategies. In long-term deployments, one could monitor the baseline and variation in the PM concentration and size in other areas of interest besides the OR and ICU, such as patient recovery rooms. These data would provide real-time data for hospital managers to assess particle distribution throughout medical facilities that can impact the exposure of patients and medical personnel to potentially infectious aerosols.

5.3.2 Application for monitoring combustion generated pollutants

There is a need for personalized exposure monitoring for susceptible individuals to help them reduce their exposure to wildfire smoke and other combustion-generated pollutants, such as

traffic emission, biomass burning, agricultural burnings, etc. Low-cost sensor networks can be utilized for both indoor and outdoor monitoring. Combustion-generated ultrafine particles (UFP) consist of elemental carbon (EC) and organic carbon (OC). Brown carbon (BrC), characterized by a significant fraction of OC, is a major air pollution component with known health risks[37] and adverse environmental impacts[38]. Size distributions, particle morphologies, optical properties, and chemical compositions of these aerosols vary significantly.[39] BrC forms from the incomplete combustion of fossil, biomass, and other carbonaceous fuels. More than 100 polycyclic aromatic hydrocarbons (PAHs) cluster to form liquid-like particles.[40] The stability of aromatic compounds is linked to the formation of soot particles.[41] The PAHs participating in PM formation or components condensed on PM during the secondary growth[42, 43] can be oxidized in the flame[44]; however, a significant organic fraction is retained by the particle, especially in the low temperature (incomplete) combustion.[45]

Climate-change-related wildfires have become more frequent and intense in the Western United States. Summer wildfire seasons are 40 to 80 days longer on average than they were 30 years ago [46]. Evidence suggests that Western states will likely see ever-worsening fires for the coming century due to climate change and land management practices [47]. The intensified wildfires will release more smoke into the atmosphere [48], traveling significant distances [49]. Fine particulate matter ($PM_{2.5}$), a significant pollutant found in smoke from wildfires, can travel deep into the respiratory tract [50]. The combustion-generated aerosols consist of elemental carbon and organic carbon fraction, which may be more toxic than other $PM_{2.5}$ sources and may have long-lasting impacts on health [51]. Complex flow structures associated with large-scale flames and low flame temperature in biomass burning lead to low carbonization of organic carbon, thus -- high levels of potentially carcinogenic polycyclic aromatic compounds [42, 44, 45]. Exposure to $PM_{2.5}$, particularly

combustion-generated aerosols, has been linked to adverse respiratory and cardiovascular health effects, including ischemic heart disease, stroke, cardiovascular mortality, and exacerbations of asthma and chronic obstructive pulmonary disease [52]

5.3.3 Addressing Low-cost Sensor Accuracy

This work utilized NaCl particles as tracer aerosols, and the calibration for a single type of aerosol can be very accurate. [19] In environmental application, the type of aerosol often varies. As low-cost sensors find applications in pollution monitoring, various studies have evaluated the performance of low-cost PM sensors in laboratory and field settings.[13, 17, 18] These reports show that low-cost sensors yield usable data when calibrated against research-grade reference instruments.[11, 19, 20] The low-cost sensor networks can provide high spatial and temporal resolution, identifying pollution sources and hotspots, which in turn can lead to the development of intervention strategies for exposure assessment and intervention strategies for susceptible individuals. Time-resolved exposure data from wearable monitors can be used to assess individual exposure in near real-time. [21]

The data accuracy from low-cost devices can come under scrutiny, and the on-site calibration can be costly, especially for large deployments [12, 35]. For example, Jiao et al. evaluated a wide variety of low-cost PM sensors; some sensors had a good agreement between identical sensors but moderate agreement with a reference PM2.5 instrument [9]. Multiple authors reported in-situ calibration and data correction strategies in the network deployment [36]. The low-cost sensor calibration studies report field-calibration accuracies R^2=0.8-0,9 [18, 53]. Specific to wildfire smoke monitoring, while new technology developments promise sensors with PM chemical specificity (mainly VOCs) [54], the current studies deploy commercially available sensors, e.g., refs [55]. There are additional considerations for stationary and wearable sensor selection. In the Siberian wildfire

monitoring study, Lin et al. reported agreement with the BAM reference instruments of R=0.94 [56], similar to our results. Liang et al. analyzed the data from PurpleAir sensor during the California wildfire season and reported good agreement with the EPA measurements (R^2=0.87) [57]. The recent EPA challenge has also demonstrated that PM type-specific calibrations improved the PM sensor accuracies to ~75–83% for conditions typical to wildfire events [58]. These studies and our results suggest that a high correlation of PMS to reference instrument for PM2.5 index can be attributed to specific correction for wildfire smoke and the dominance of these PM in the airshed during the wildfire. Over if low-cost sensors are used for environmental monitoring, one needs to be aware of sensor calibration. These can be achieved by pre- and post-evaluation of sensor performance in a controlled environment, such as aerosol test chamber control for humidity, particle size, and concentration levels.[59]

6 Chapter 6: Conclusions

6.1 Conclusions

The use of the sensor network measurements informed the development of a reduced-order zonal model for aerosol distribution in ORs and ICUs. Evidence-based intervention strategies can be developed for specific environments using this sensor network. We were able to model each room as three distinct zones and generalize this pattern throughout each experiment, demonstrating that this procedure is generalizable and expandable and can be used in many applications, including other hospital environments (such as emergency departments) or non-healthcare areas such as gyms, restaurants, schools, and office buildings.

In the OR experiments, we could see that nearly all the aerosol stayed at the bed and very little dispersed to the perimeter or outside of the room. The ORs never became well-mixed, and

therefore fitting a decay rate to each OR did not work well since the room had spatial variation in PM concentration and the rooms varied in size: between 110m^3 and 250m^3. The ICUs were almost identical in size and shape and showed less variability between experiments. For future experiments in ORs, it would be worth repeating experiments with a 5-minute aerosolization period as we saw during the trial at HMC, in which the OR reached a well-mixed state, which would allow for decay rate analysis.

We demonstrated that negative pressure rooms were effective in controlling aerosol release in ICUs. Negative pressure ICUs clear aerosols to background levels up to 1.5-2 times faster positive-pressure room. Negative pressure rooms also control aerosol leaks, generated PM stayed in the room and was evacuated by the HVAC, while in neutral or positive pressure rooms, up to 18% of the aerosol escaped to outside areas. Neutral pressure rooms consistently had the worst aerosol exfiltration, suggesting that shutting an ICU door could aid in aerosol control. We demonstrated that dividing the sensors into zones using unsupervised learning in Python gave similar results to the zones found by diving the room into zones spatially based on the proximity to the aerosolization source. Though the zoning methods did not affect decay rate analysis, the k-means method can determine dead zones and aerosol release zones without *a priori* assumptions.

References

(1) Foocharoen, C.; Peansukwech, U.; Pongkulkiat, P.; Mahakkanukrauh, A.; Suwannaroj, S. Aerosol components associated with hospital mortality in systemic sclerosis: an analysis from a nationwide Thailand healthcare database. *Scientific Reports* **2021**, *11* (1). DOI: 10.1038/s41598-021-87114-0 (acccessed 2021-07-26T09:57:32). Fabian, P.; Mcdevitt, J. J.; Dehaan, W. H.; Fung, R. O. P.; Cowling, B. J.; Chan, K. H.; Leung, G. M.; Milton, D. K. Influenza Virus in Human Exhaled Breath: An Observational Study. *PLoS ONE* **2008**, *3* (7), e2691. DOI: 10.1371/journal.pone.0002691 (acccessed 2021-07-12T06:40:14). Cowling, B. J.; Ip, D. K. M.; Fang, V. J.; Suntarattiwong, P.; Olsen, S. J.; Levy, J.; Uyeki, T. M.; Leung, G. M.; Malik Peiris, J. S.; Chotpitayasunondh, T.; et al. Aerosol transmission is an important mode of influenza A virus spread. *Nature Communications* **2013**, *4* (1). DOI: 10.1038/ncomms2922 (acccessed 2021-07-26T09:47:53). Pandey, N.; Basnet, B. B.; Koju, S.; Khapung, A.; Gupta, A. Awareness of aerosol-related transmission of COVID-19 among the dentists of Nepal. *BDJ Open* **2021**, *7* (1). DOI: 10.1038/s41405-021-00079-0 (acccessed 2021-07-26T10:00:13). Tang, S.; Mao, Y.; Jones, R. M.; Tan, Q.; Ji, J. S.; Li, N.; Shen, J.; Lv, Y.; Pan, L.; Ding, P.; et al. Aerosol transmission of SARS-CoV-2? Evidence, prevention and control. *Environment International* **2020**, *144*, 106039. DOI: 10.1016/j.envint.2020.106039 (acccessed 2021-05-12T18:42:38). Mürbe, D.; Kriegel, M.; Lange, J.; Rotheudt, H.; Fleischer, M. Aerosol emission in professional singing of classical music. *Scientific Reports* **2021**, *11* (1). DOI: 10.1038/s41598-021-93281-x (acccessed 2021-07-26T09:52:30). Tian, J.; Wang, Q.; Zhang, Y.; Yan, M.; Liu, H.; Zhang, N.; Ran, W.; Cao, J. Impacts of primary emissions and secondary aerosol formation on air pollution in an urban area of China during the COVID-19 lockdown. *Environment International* **2021**, *150*, 106426. DOI: 10.1016/j.envint.2021.106426 (acccessed 2021-12-03T01:34:56). Kumar, P.; Omidvarborna, H.; Tiwari, A.; Morawska, L. The nexus between in-car aerosol concentrations, ventilation and the risk of respiratory infection. *Environment International* **2021**, *157*, 106814. DOI: 10.1016/j.envint.2021.106814 (acccessed 2021-12-03T01:37:34).
(2) Guo, Z.-D.; Wang, Z.-Y.; Zhang, S.-F.; Li, X.; Li, L.; Li, C.; Cui, Y.; Fu, R.-B.; Dong, Y.-Z.; Chi, X.-Y.; et al. Aerosol and Surface Distribution of Severe Acute Respiratory Syndrome Coronavirus 2 in Hospital Wards, Wuhan, China, 2020. *Emerging Infectious Diseases* **2020**, *26* (7), 1583-1591. DOI: 10.3201/eid2607.200885 (acccessed 2021-07-12T08:20:16).
(3) Jin, T.; Li, J.; Yang, J.; Li, J.; Hong, F.; Long, H.; Deng, Q.; Qin, Y.; Jiang, J.; Zhou, X.; et al. SARS-CoV-2 presented in the air of an intensive care unit (ICU). *Sustainable Cities and Society* **2021**, *65*. DOI: 10.1016/j.scs.2020.102446.
(4) Gogate, U.; Bakal, J. W. Smart Healthcare Monitoring System based on Wireless Sensor Networks. In *2016 International Conference on Computing, Analytics and Security Trends (CAST)*, 2016-12-01, 2016; IEEE. DOI: 10.1109/cast.2016.7915037. Silva, R.; Silva, J. S.; Silva, A.; Pinto, F. C.; Simek, M.; Boavida, F. Wireless Sensor Networks in Intensive Care Units. In *2009 IEEE International Conference on Communications Workshops*, 2009-06-01, 2009; IEEE. DOI: 10.1109/iccw.2009.5208086. Liu, Y.; Ning, Z.; Chen, Y.; Guo, M.; Liu, Y.; Gali, N. K.; Sun, L.; Duan, Y.; Cai, J.; Westerdahl, D.; et al. Aerodynamic analysis of SARS-CoV-2 in two Wuhan hospitals. *Nature* **2020**, *582* (7813), 557-560. DOI: 10.1038/s41586-020-2271-3 (acccessed 2021-07-26T10:03:59). Crawford, C.; Vanoli, E.; Decorde, B.; Lancelot, M.; Duprat, C.; Josserand, C.; Jilesen, J.; Bouadma, L.; Timsit, J.-F. Modeling of aerosol transmission of airborne pathogens in ICU rooms of COVID-19 patients with acute respiratory failure. *Scientific Reports* **2021**, *11* (1). DOI: 10.1038/s41598-021-91265-5 (acccessed 2021-07-08T22:28:02).
(5) Stieglitz, S. The ICU. In *Covid-19 Airway Management and Ventilation Strategy for Critically Ill Older Patients*, Springer International Publishing, 2020; pp 183-188. Ong, S. W. X.; Lee, P. H.; Tan, Y. K.; Ling, L. M.; Ho, B. C. H.; Ng, C. G.; Wang, D. L.; Tan, B. H.; Leo, Y.-S.; Ng, O.-T.; et al. Environmental contamination in a coronavirus disease 2019 (COVID-19) intensive care unit—What is the risk? *Infection*

Control & Hospital Epidemiology **2021**, *42* (6), 669-677. DOI: 10.1017/ice.2020.1278 (acccessed 2021-07-12T08:48:58).
(6) Makhsous, S.; Segovia, J. M.; He, J.; Chan, D.; Lee, L.; Novosselov, I. V.; Mamishev, A. V. Methodology for Addressing Infectious Aerosol Persistence in Real-Time Using Sensor Network. *Sensors* **2021**, *21* (11), 3928.
(7) Hegde, S.; Min, K. T.; Moore, J.; Lundrigan, P.; Patwari, N.; Collingwood, S.; Balch, A.; Kelly, K. E. Indoor household particulate matter measurements using a network of low-cost sensors. *Aerosol and Air Quality Research* **2020**, *20* (2), 381-394. Li, J.; Li, H.; Ma, Y.; Wang, Y.; Abokifa, A. A.; Lu, C.; Biswas, P. Spatiotemporal distribution of indoor particulate matter concentration with a low-cost sensor network. *Building and Environment* **2018**, *127*, 138-147. Kumar, P.; Skouloudis, A. N.; Bell, M.; Viana, M.; Carotta, M. C.; Biskos, G.; Morawska, L. Real-time sensors for indoor air monitoring and challenges ahead in deploying them to urban buildings. *Science of the Total Environment* **2016**, *560*, 150-159.
(8) Seto, E.; Austin, E.; Novosselov, I.; Yost, M. G. Use of low-cost particle monitors to calibrate traffic-related air pollutant models in urban areas. In *International Environmental Modelling and Software Society*, 2014. Liu, X.; Jayaratne, R.; Thai, P.; Kuhn, T.; Zing, I.; Christensen, B.; Lamont, R.; Dunbabin, M.; Zhu, S.; Gao, J. Low-cost sensors as an alternative for long-term air quality monitoring. *Environmental research* **2020**, *185*, 109438. Kuhn, T.; Jayaratne, R.; Thai, P. K.; Christensen, B.; Liu, X.; Dunbabin, M.; Lamont, R.; Zing, I.; Wainwright, D.; Witte, C. Air quality during and after the Commonwealth Games 2018 in Australia: Multiple benefits of monitoring. *Journal of Aerosol Science* **2021**, *152*, 105707. Gao, M.; Cao, J.; Seto, E. A distributed network of low-cost continuous reading sensors to measure spatiotemporal variations of PM2.5 in Xi'an, China. *Environmental Pollution* **2015**, *199*, 56-65. DOI: http://dx.doi.org/10.1016/j.envpol.2015.01.013.
(9) Jiao, W.; Hagler, G.; Williams, R.; Sharpe, R.; Brown, R.; Garver, D.; Judge, R.; Caudill, M.; Rickard, J.; Davis, M. Community Air Sensor Network (CAIRSENSE) project: evaluation of low-cost sensor performance in a suburban environment in the southeastern United States. *Atmospheric Measurement Techniques* **2016**, *9* (11), 5281-5292.
(10) Kumar, P.; Morawska, L.; Martani, C.; Biskos, G.; Neophytou, M.; Di Sabatino, S.; Bell, M.; Norford, L.; Britter, R. The rise of low-cost sensing for managing air pollution in cities. *Environment international* **2015**, *75*, 199-205. Li, J.; Zhang, H.; Chao, C.-Y.; Chien, C.-H.; Wu, C.-Y.; Luo, C. H.; Chen, L.-J.; Biswas, P. Integrating low-cost air quality sensor networks with fixed and satellite monitoring systems to study ground-level PM2. 5. *Atmospheric Environment* **2020**, *223*, 117293.
(11) Chao, C.-Y.; Zhang, H.; Hammer, M.; Zhan, Y.; Kenney, D.; Martin, R. V.; Biswas, P. Integrating Fixed Monitoring Systems with Low-Cost Sensors to Create High-Resolution Air Quality Maps for the Northern China Plain Region. *ACS Earth and Space Chemistry* **2021**, *5* (11), 3022-3035.
(12) Qiao, X.; Zhang, Q.; Wang, D.; Hao, J.; Jiang, J. Improving data reliability: A quality control practice for low-cost PM2. 5 sensor network. *Science of The Total Environment* **2021**, *779*, 146381.
(13) Austin, E.; Novosselov, I.; Seto, E.; Yost, M. G. Laboratory Evaluation of the Shinyei PPD42NS Low-Cost Particulate Matter Sensor. *PloS one* **2015**, *10* (9), e0137789.
(14) Sousan, S.; Koehler, K.; Thomas, G.; Park, J. H.; Hillman, M.; Halterman, A.; Peters, T. M. Inter-comparison of low-cost sensors for measuring the mass concentration of occupational aerosols. *Aerosol Science and Technology* **2016**, *50* (5), 462-473. DOI: 10.1080/02786826.2016.1162901.
(15) Njalsson, T.; Novosselov, I. Design and optimization of a compact low-cost optical particle sizer. *Journal of Aerosol Science* **2018**, *119*, 1-12.
(16) Renard, J.-B.; Dulac, F.; Berthet, G.; Lurton, T.; Vignelles, D.; Jégou, F.; Tonnelier, T.; Jeannot, M.; Couté, B.; Akiki, R. LOAC: a small aerosol optical counter/sizer for ground-based and balloon measurements of the size distribution and nature of atmospheric particles–Part 2: First results from balloon and unmanned aerial vehicle flights. *Atmospheric Measurement Techniques* **2016**, *9* (8), 3673-3686. Nagy, A.; Szymanski, W.; Gal, P.; Golczewski, A.; Czitrovszky, A. Numerical and experimental study

of the performance of the dual wavelength optical particle spectrometer (DWOPS). *Journal of aerosol science* **2007**, *38* (4), 467-478.
(17) Cordero, J. M.; Borge, R.; Narros, A. Using statistical methods to carry out in field calibrations of low cost air quality sensors. *Sensors and Actuators B: Chemical* **2018**, *267*, 245-254. Feenstra, B.; Papapostolou, V.; Hasheminassab, S.; Zhang, H.; Der Boghossian, B.; Cocker, D.; Polidori, A. Performance evaluation of twelve low-cost PM2. 5 sensors at an ambient air monitoring site. *Atmospheric Environment* **2019**, *216*, 116946. Sayahi, T.; Butterfield, A.; Kelly, K. Long-term field evaluation of the Plantower PMS low-cost particulate matter sensors. *Environmental pollution* **2019**, *245*, 932-940. Tryner, J.; L'Orange, C.; Mehaffy, J.; Miller-Lionberg, D.; Hofstetter, J. C.; Wilson, A.; Volckens, J. Laboratory evaluation of low-cost PurpleAir PM monitors and in-field correction using co-located portable filter samplers. *Atmospheric Environment* **2020**, *220*, 117067. Wang, Z.; Delp, W. W.; Singer, B. C. Performance of low-cost indoor air quality monitors for PM2. 5 and PM10 from residential sources. *Building and Environment* **2020**, *171*, 106654. Zusman, M.; Schumacher, C. S.; Gassett, A. J.; Spalt, E. W.; Austin, E.; Larson, T. V.; Carvlin, G.; Seto, E.; Kaufman, J. D.; Sheppard, L. Calibration of low-cost particulate matter sensors: Model development for a multi-city epidemiological study. *Environment International* **2020**, *134*, 105329.
(18) Kelly, K.; Whitaker, J.; Petty, A.; Widmer, C.; Dybwad, A.; Sleeth, D.; Martin, R.; Butterfield, A. Ambient and laboratory evaluation of a low-cost particulate matter sensor. *Environmental pollution* **2017**, *221*, 491-500.
(19) Huang, C.-H.; He, J.; Austin, E.; Seto, E.; Novosselov, I. Assessing the value of complex refractive index and particle density for calibration of low-cost particle matter sensor for size-resolved particle count and PM2. 5 measurements. *Plos one* **2021**, *16* (11), e0259745.
(20) Li, J.; Mattewal, S. K.; Patel, S.; Biswas, P. Evaluation of nine low-cost-sensor-based particulate matter monitors. *Aerosol and Air Quality Research* **2020**, *20* (2), 254-270.
(21) Duncan, G. E.; Seto, E.; Avery, A. R.; Oie, M.; Carvlin, G.; Austin, E.; Shirai, J. H.; He, J.; Ockerman, B.; Novosselov, I. Usability of a personal air pollution monitor: Design-feedback iterative cycle study. *JMIR mHealth and uHealth* **2018**, *6* (12), e12023.
(22) He, J.; Huang, C.-H.; Yuan, N.; Austin, E.; Seto, E.; Novosselov, I. Network of Low-cost Air Quality Sensor for Monitoring Indoor, Outdoor, and Personal PM2.5 Exposure in Seattle during the 2020 Wildfire Season. 2021.
(23) Bontempi, G.; Le Borgne, Y. An adaptive modular approach to the mining of sensor network data. In *proceedings of 1st International Workshop on Data Mining in Sensor Networks as part of the SIAM International Conference on Data Mining*, 2005; SIAM Press Newport Beach, CA: pp 3-9.
(24) Akyildiz, I. F.; Su, W.; Sankarasubramaniam, Y.; Cayirci, E. A survey on sensor networks. *IEEE Communications Magazine* **2002**, *40* (8), 102-114. DOI: 10.1109/mcom.2002.1024422 (acccessed 2022-01-14T16:47:10).
(25) Harb, H.; Makhoul, A.; Laiymani, D.; Jaber, A.; Tawil, R. K-means based clustering approach for data aggregation in periodic sensor networks. In *2014 IEEE 10th International Conference on Wireless and Mobile Computing, Networking and Communications (WiMob)*, 2014-10-01, 2014; IEEE. DOI: 10.1109/wimob.2014.6962207. Hua, M.; Lau, M. K.; Pei, J.; Wu, K. Continuous K-Means Monitoring with Low Reporting Cost in Sensor Networks. *IEEE Transactions on Knowledge and Data Engineering* **2009**, *21* (12), 1679-1691. DOI: 10.1109/tkde.2009.41 (acccessed 2022-01-14T17:27:54).
(26) Sasikumar, P.; Khara, S. K-Means Clustering in Wireless Sensor Networks. In *2012 Fourth International Conference on Computational Intelligence and Communication Networks*, 2012-11-01, 2012; IEEE. DOI: 10.1109/cicn.2012.136.
(27) Tang, J. W.; Marr, L. C.; Li, Y.; Dancer, S. J. Covid-19 has redefined airborne transmission. *BMJ* **2021**, n913. DOI: 10.1136/bmj.n913 (acccessed 2021-11-17T02:18:51). Allen, J. G.; Ibrahim, A. M. Indoor Air

Changes and Potential Implications for SARS-CoV-2 Transmission. *JAMA* **2021**, *325* (20), 2112. DOI: 10.1001/jama.2021.5053 (acccessed 2022-02-17T21:40:56).
(28) Morawska, L.; Allen, J.; Bahnfleth, W.; Bluyssen, P. M.; Boerstra, A.; Buonanno, G.; Cao, J.; Dancer, S. J.; Floto, A.; Franchimon, F.; et al. A paradigm shift to combat indoor respiratory infection. *Science* **2021**, *372* (6543), 689-691. DOI: 10.1126/science.abg2025 (acccessed 2021-05-19T01:12:15).
(29) Elred, S. New OSHA Standards Are Coming for COVID-19. Better Late Than Never? Medscape: 2021.
(30) Crilley, L. R.; Shaw, M.; Pound, R.; Kramer, L. J.; Price, R.; Young, S.; Lewis, A. C.; Pope, F. D. Evaluation of a low-cost optical particle counter (Alphasense OPC-N2) for ambient air monitoring. *Atmospheric Measurement Techniques* **2018**, *11* (2), 709-720.
(31) Czitrovszky, A. Environmental applications of solid-state lasers. In *Handbook of Solid-State Lasers*, Elsevier, 2013; pp 616-646.
(32) Lee, B. U. Minimum Sizes of Respiratory Particles Carrying SARS-CoV-2 and the Possibility of Aerosol Generation. *International Journal of Environmental Research and Public Health* **2020**, *17* (19), 6960. DOI: 10.3390/ijerph17196960 (acccessed 2021-07-23T16:56:21). Pastuszka, J. S.; Kyaw Tha Paw, U.; Lis, D. O.; Wlazło, A.; Ulfig, K. Bacterial and fungal aerosol in indoor environment in Upper Silesia, Poland. *Atmospheric Environment* **2000**, *34* (22), 3833-3842. DOI: 10.1016/s1352-2310(99)00527-0 (acccessed 2021-12-03T01:28:47).
(33) Vaddi, R. S.; Guan, Y.; Novosselov, I. Behavior of ultrafine particles in electro-hydrodynamic flow induced by corona discharge. *Journal of Aerosol Science* **2020**, *148*, 105587. DOI: 10.1016/j.jaerosci.2020.105587 (acccessed 2021-07-23T07:18:35).
(34) Glenn, K.; He, J.; Rochlin, R.; Teng, S.; Hecker, J.; Novosselov, I. Zonal Model of Aerosol Persistence in ICUs: Utilization of Time and Space-resolved Sensor Network. *medRxiv* **2022**.
(35) Moltchanov, S.; Levy, I.; Etzion, Y.; Lerner, U.; Broday, D. M.; Fishbain, B. On the feasibility of measuring urban air pollution by wireless distributed sensor networks. *Science of The Total Environment* **2015**, *502*, 537-547.
(36) Si, M.; Xiong, Y.; Du, S.; Du, K. Evaluation and calibration of a low-cost particle sensor in ambient conditions using machine-learning methods. *Atmospheric Measurement Techniques* **2020**, *13* (4), 1693-1707. Miskell, G.; Salmond, J. A.; Williams, D. E. Solution to the problem of calibration of low-cost air quality measurement sensors in networks. *ACS sensors* **2018**, *3* (4), 832-843. Topalović, D. B.; Davidović, M. D.; Jovanović, M.; Bartonova, A.; Ristovski, Z.; Jovašević-Stojanović, M. In search of an optimal in-field calibration method of low-cost gas sensors for ambient air pollutants: Comparison of linear, multilinear and artificial neural network approaches. *Atmospheric Environment* **2019**, *213*, 640-658. Datta, A.; Saha, A.; Zamora, M. L.; Buehler, C.; Hao, L.; Xiong, F.; Gentner, D. R.; Koehler, K. Statistical field calibration of a low-cost PM2. 5 monitoring network in Baltimore. *Atmospheric Environment* **2020**, *242*, 117761. Delaine, F.; Lebental, B.; Rivano, H. In situ calibration algorithms for environmental sensor networks: A review. *IEEE Sensors Journal* **2019**, *19* (15), 5968-5978. Hofman, J.; Nikolaou, M.; Shantharam, S. P.; Stroobants, C.; Weijs, S.; La Manna, V. P. Distant calibration of low-cost PM and NO2 sensors; evidence from multiple sensor testbeds. *Atmospheric Pollution Research* **2022**, *13* (1), 101246. Kosmopoulos, G.; Salamalikis, V.; Pandis, S.; Yannopoulos, P.; Bloutsos, A.; Kazantzidis, A. Low-cost sensors for measuring airborne particulate matter: Field evaluation and calibration at a South-Eastern European site. *Science of The Total Environment* **2020**, *748*, 141396. Zimmerman, N. Tutorial: Guidelines for implementing low-cost sensor networks for aerosol monitoring. *Journal of Aerosol Science* **2022**, *159*, 105872. Wallace, L.; Bi, J.; Ott, W. R.; Sarnat, J.; Liu, Y. Calibration of low-cost PurpleAir outdoor monitors using an improved method of calculating PM2. 5. *Atmospheric Environment* **2021**, *256*, 118432.
(37) Peters, A.; Veronesi, B.; Calderón-Garcidueñas, L.; Gehr, P.; Chen, L. C.; Geiser, M.; Reed, W.; Rothen-Rutishauser, B.; Schürch, S.; Schulz, H. Translocation and potential neurological effects of fine and ultrafine particles a critical update. *Particle and fibre toxicology* **2006**, *3* (1), 13.

(38) Fuzzi, S.; Baltensperger, U.; Carslaw, K.; Decesari, S.; Denier Van Der Gon, H.; Facchini, M.; Fowler, D.; Koren, I.; Langford, B.; Lohmann, U. Particulate matter, air quality and climate: lessons learned and future needs. *Atmospheric chemistry and physics* **2015**, *15* (14), 8217-8299.
(39) Elbayoumi, M.; Ramli, N. A.; Md Yusof, N. F. F. Spatial and temporal variations in particulate matter concentrations in twelve schools environment in urban and overpopulated camps landscape. *Building and Environment* **2015**, *90*, 157-167. DOI: http://dx.doi.org/10.1016/j.buildenv.2015.03.036. Patel, M. M.; Chillrud, S. N.; Correa, J. C.; Feinberg, M.; Hazi, Y.; Kc, D.; Prakash, S.; Ross, J. M.; Levy, D.; Kinney, P. L. Spatial and Temporal Variations in Traffic-related Particulate Matter at New York City High Schools. *Atmospheric environment (Oxford, England : 1994)* **2009**, *43* (32), 4975-4981. DOI: 10.1016/j.atmosenv.2009.07.004 PMC.
(40) Dobbins, R. A. Soot inception temperature and the carbonization rate of precursor particles. *Combustion and Flame* **2002**, *130* (3), 204-214.
(41) Stein, S. E.; Fahr, A. High-temperature stabilities of hydrocarbons. *The Journal of Physical Chemistry* **1985**, *89* (17), 3714-3725. Commodo, M.; Kaiser, K.; De Falco, G.; Minutolo, P.; Schulz, F.; D'Anna, A.; Gross, L. On the early stages of soot formation: Molecular structure elucidation by high-resolution atomic force microscopy. *Combustion and Flame* **2019**, *205*, 154-164.
(42) Davis, J.; Tiwari, K.; Novosselov, I. Soot morphology and nanostructure in complex flame flow patterns via secondary particle surface growth. *Fuel* **2019**, *245*, 447-457. DOI: https://doi.org/10.1016/j.fuel.2019.02.058.
(43) Davis, J. Characterization of combustion generated particulates produced in an inverted gravity flame reactor University of Washington, Seattle, 2019.
(44) West, C. P.; Hettiyadura, A. P. S.; Darmody, A.; Mahamuni, G.; Davis, J.; Novosselov, I.; Laskin, A. Molecular Composition and the Optical Properties of Brown Carbon Generated by the Ethane Flame. *ACS Earth and Space Chemistry* **2020**, *4* (7), 1090-1103. DOI: 10.1021/acsearthspacechem.0c00095. Davis, J.; Molnar, E.; Novosselov, I. Nanostructure transition of young soot aggregates to mature soot aggregates in diluted diffusion flames. *Carbon* **2020**, *159*, 255-265. DOI: https://doi.org/10.1016/j.carbon.2019.12.043.
(45) Mahamuni, G.; Rutherford, J.; Davis, J.; Molnar, E.; Posner, J. D.; Seto, E.; Korshin, G.; Novosselov, I. Excitation–Emission Matrix Spectroscopy for Analysis of Chemical Composition of Combustion Generated Particulate Matter. *Environmental Science & Technology* **2020**, *54* (13), 8198-8209. DOI: 10.1021/acs.est.0c01110.
(46) Jolly, W. M.; Cochrane, M. A.; Freeborn, P. H.; Holden, Z. A.; Brown, T. J.; Williamson, G. J.; Bowman, D. M. J. S. Climate-induced variations in global wildfire danger from 1979 to 2013. *Nature Communications* **2015**, *6* (1), 7537. DOI: 10.1038/ncomms8537 (acccessed 2021-08-02T20:59:02).
(47) Kennedy, M. C.; Bart, R. R.; Tague, C. L.; Choate, J. S. Does hot and dry equal more wildfire? Contrasting short- and long-term climate effects on fire in the Sierra Nevada, CA. *Ecosphere* **2021**, *12* (7). DOI: 10.1002/ecs2.3657 (acccessed 2021-08-02T00:23:01). Barbero, R.; Abatzoglou, J. T.; Larkin, N. K.; Kolden, C. A.; Stocks, B. Climate change presents increased potential for very large fires in the contiguous United States. *International Journal of Wildland Fire* **2015**, *24* (7), 892. DOI: 10.1071/wf15083 (acccessed 2021-08-02T06:41:59). Spracklen, D. V.; Mickley, L. J.; Logan, J. A.; Hudman, R. C.; Yevich, R.; Flannigan, M. D.; Westerling, A. L. Impacts of climate change from 2000 to 2050 on wildfire activity and carbonaceous aerosol concentrations in the western United States. *Journal of Geophysical Research* **2009**, *114* (D20). DOI: 10.1029/2008jd010966 (acccessed 2021-08-02T06:48:23). Burke, M.; Driscoll, A.; Heft-Neal, S.; Xue, J.; Burney, J.; Wara, M. The changing risk and burden of wildfire in the United States. *Proceedings of the National Academy of Sciences* **2021**, *118* (2).
(48) Yue, X.; Mickley, L. J.; Logan, J. A.; Kaplan, J. O. Ensemble projections of wildfire activity and carbonaceous aerosol concentrations over the western United States in the mid-21st century.

Atmospheric Environment **2013**, *77*, 767-780. DOI: 10.1016/j.atmosenv.2013.06.003 (acccessed 2021-08-02T06:52:11).
(49) Tiwari, S.; Dumka, U.; Gautam, A.; Kaskaoutis, D.; Srivastava, A.; Bisht, D.; Chakrabarty, R.; Sumlin, B.; Solmon, F. Assessment of PM2. 5 and PM10 over Guwahati in Brahmaputra River Valley: Temporal evolution, source apportionment and meteorological dependence. *Atmospheric Pollution Research* **2017**, *8* (1), 13-28.
(50) Burke, M.; Driscoll, A.; Heft-Neal, S.; Xue, J.; Burney, J.; Wara, M. The changing risk and burden of wildfire in the United States. *Proceedings of the National Academy of Sciences* **2021**, *118* (2), e2011048118. DOI: 10.1073/pnas.2011048118 (acccessed 2021-07-08T19:03:10).
(51) Samburova, V.; Zielinska, B.; Khlystov, A. Do 16 polycyclic aromatic hydrocarbons represent PAH air toxicity? *Toxics* **2017**, *5* (3), 17. Aguilera, R.; Corringham, T.; Gershunov, A.; Benmarhnia, T. Wildfire smoke impacts respiratory health more than fine particles from other sources: observational evidence from Southern California. *Nature Communications* **2021**, *12* (1). DOI: ARTN 1493 10.1038/s41467-021-21708-0. Magzamen, S.; Gan, R. W.; Liu, J. Y.; O'Dell, K.; Ford, B.; Berg, K.; Bol, K.; Wilson, A.; Fischer, E. V.; Pierce, J. R. Differential Cardiopulmonary Health Impacts of Local and Long-Range Transport of Wildfire Smoke. *Geohealth* **2021**, *5* (3). DOI: ARTN e2020GH000330 10.1029/2020GH000330. Landguth, E. L.; Holden, Z. A.; Graham, J.; Stark, B.; Mokhtari, E. B.; Kaleczyc, E.; Anderson, S.; Urbanski, S.; Jolly, M.; Semmens, E. O.; et al. The delayed effect of wildfire season particulate matter on subsequent influenza season in a mountain west region of the USA. *Environment International* **2020**, *139*. DOI: ARTN 105668 10.1016/j.envint.2020.105668.
(52) Deflorio-Barker, S.; Crooks, J.; Reyes, J.; Rappold, A. G. Cardiopulmonary Effects of Fine Particulate Matter Exposure among Older Adults, during Wildfire and Non-Wildfire Periods, in the United States 2008–2010. *Environmental Health Perspectives* **2019**, *127* (3), 037006. DOI: 10.1289/ehp3860 (acccessed 2021-08-02T01:27:12). Liu, Y.; Austin, E.; Xiang, J.; Gould, T.; Larson, T.; Seto, E. Health Impact Assessment of the 2020 Washington State Wildfire Smoke Episode: Excess Health Burden Attributable to Increased $PM_{2.5}$ Exposures and Potential Exposure Reductions. *GeoHealth* **2021**, *5* (5). DOI: 10.1029/2020gh000359 (acccessed 2021-06-22T21:07:54). Dennekamp, M.; Abramson, M. J. The effects of bushfire smoke on respiratory health. *Respirology* **2011**, *16* (2), 198-209. DOI: 10.1111/j.1440-1843.2010.01868.x (acccessed 2021-08-02T01:08:27). Reid, C. E.; Brauer, M.; Johnston, F. H.; Jerrett, M.; Balmes, J. R.; Elliott, C. T. Critical review of health impacts of wildfire smoke exposure. *Environmental health perspectives* **2016**, *124* (9), 1334-1343. Matz, C. J.; Egyed, M.; Xi, G.; Racine, J.; Pavlovic, R.; Rittmaster, R.; Henderson, S. B.; Stieb, D. M. Health impact analysis of PM2. 5 from wildfire smoke in Canada (2013–2015, 2017–2018). *Science of the Total Environment* **2020**, *725*, 138506.
(53) Levy Zamora, M.; Xiong, F.; Gentner, D.; Kerkez, B.; Kohrman-Glaser, J.; Koehler, K. Field and laboratory evaluations of the low-cost plantower particulate matter sensor. *Environmental science & technology* **2018**, *53* (2), 838-849. Zamora, M. L.; Xiong, F. L. Z.; Gentner, D.; Kerkez, B.; Kohrman-Glaser, J.; Koehler, K. Field and Laboratory Evaluations of the Low-Cost Plantower Particulate Matter Sensor. *Environmental Science & Technology* **2019**, *53* (2), 838-849. DOI: 10.1021/acs.est.8b05174.
(54) Lin, E. Z.; Esenther, S.; Mascelloni, M.; Irfan, F.; Godri Pollitt, K. J. The fresh air wristband: A wearable air pollutant sampler. *Environmental Science & Technology Letters* **2020**, *7* (5), 308-314. Mahamuni, G.; He, J.; Rutherford, J.; Ockerman, B.; Majumdar, A.; Seto, E.; Korshin, G.; Novosselov, I. Solid-phase excitation-emission matrix spectroscopy for chemical analysis of combustion aerosols. *PloS one* **2021**, *16* (5), e0251664. Fung, A. G.; Rajapakse, M. Y.; McCartney, M. M.; Falcon, A. K.; Fabia, F. M.; Kenyon, N. J.; Davis, C. E. Wearable environmental monitor to quantify personal ambient volatile organic compound exposures. *ACS sensors* **2019**, *4* (5), 1358-1364. Rajapakse, M. Y.; Borras, E.; Fung, A. G.; Yeap, D.; McCartney, M. M.; Fabia, F. M.; Kenyon, N. J.; Davis, C. E. An environmental air sampler to evaluate personal exposure to volatile organic compounds. *Analyst* **2021**, *146* (2), 636-645.

(55) Holder, A. L.; Mebust, A. K.; Maghran, L. A.; McGown, M. R.; Stewart, K. E.; Vallano, D. M.; Elleman, R. A.; Baker, K. R. Field evaluation of low-cost particulate matter sensors for measuring wildfire smoke. *Sensors* **2020**, *20* (17), 4796. Stampfer, O.; Austin, E.; Ganuelas, T.; Fiander, T.; Seto, E.; Karr, C. J. Use of low-cost PM monitors and a multi-wavelength aethalometer to characterize PM2. 5 in the Yakama Nation reservation. *Atmospheric Environment* **2020**, *224*, 117292.
(56) Lin, C.; Labzovskii, L. D.; Mak, H. W. L.; Fung, J. C.; Lau, A. K.; Kenea, S. T.; Bilal, M.; Hey, J. D. V.; Lu, X.; Ma, J. Observation of PM2. 5 using a combination of satellite remote sensing and low-cost sensor network in Siberian urban areas with limited reference monitoring. *Atmospheric Environment* **2020**, *227*, 117410.
(57) Liang, Y.; Sengupta, D.; Campmier, M. J.; Lunderberg, D. M.; Apte, J. S.; Goldstein, A. H. Wildfire smoke impacts on indoor air quality assessed using crowdsourced data in California. *Proceedings of the National Academy of Sciences* **2021**, *118* (36).
(58) Landis, M. S.; Long, R. W.; Krug, J.; Colón, M.; Vanderpool, R.; Habel, A.; Urbanski, S. P. The US EPA wildland fire sensor challenge: Performance and evaluation of solver submitted multi-pollutant sensor systems. *Atmospheric Environment* **2021**, *247*, 118165.
(59) He, J. Y.; Novosselov, I. V. Design and evaluation of an aerodynamic focusing micro-well aerosol collector. *Aerosol Science and Technology* **2017**, *51* (9), 1016-1026. DOI: 10.1080/02786826.2017.1329515. Zhang, J.; Dichiara, A. B.; Novosselov, I.; Gao, D.; Chung, J.-H. Polyacrylic acid coated carbon nanotube–paper composites for humidity and moisture sensing. *Journal of Materials Chemistry C* **2019**, *7* (18), 5374-5380. He, J.; Beck, N. K.; Kossik, A. L.; Zhang, J.; Seto, E.; Meschke, J. S.; Novosselov, I. Evaluation of micro-well collector for capture and analysis of aerosolized Bacillus subtilis spores. *PloS one* **2018**, *13* (5), e0197783.

Appendix

In Supplementary Figure 1, the average of all the sensors is shown with a curve-fitted line to show the decay rate. In the first two, the decay rate is not accurate because it does not have a consistent starting point or ending point since the data is never clearly linear, but in the third experiment, when all the zones become well-mixed and show the same decay rate, there is a much clearer and more accurate decay rate for the whole room.

OR	Blocked	Unblocked
OR 5	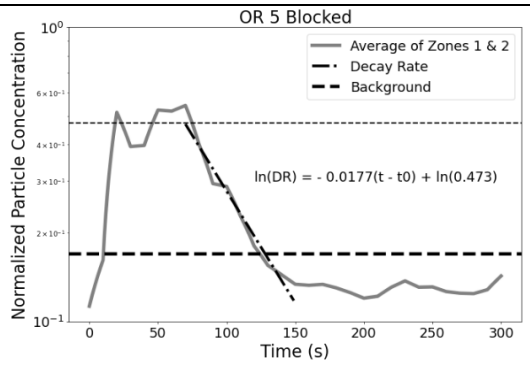	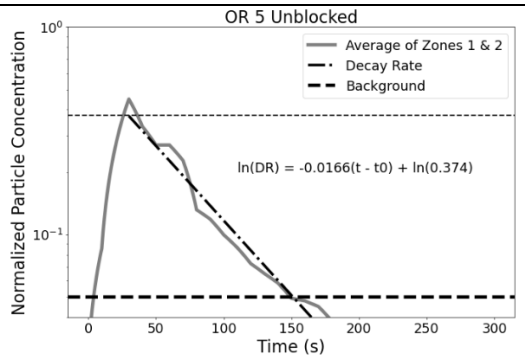
OR 7	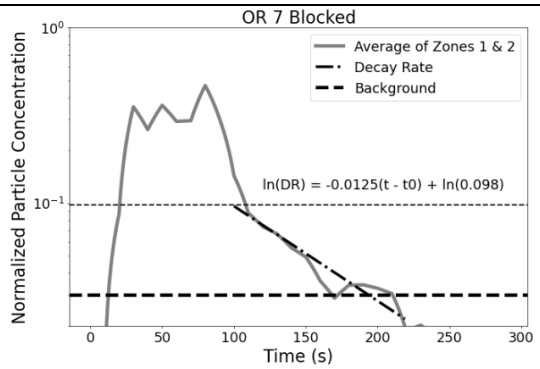	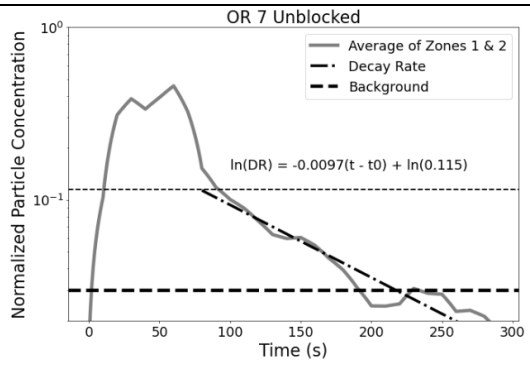

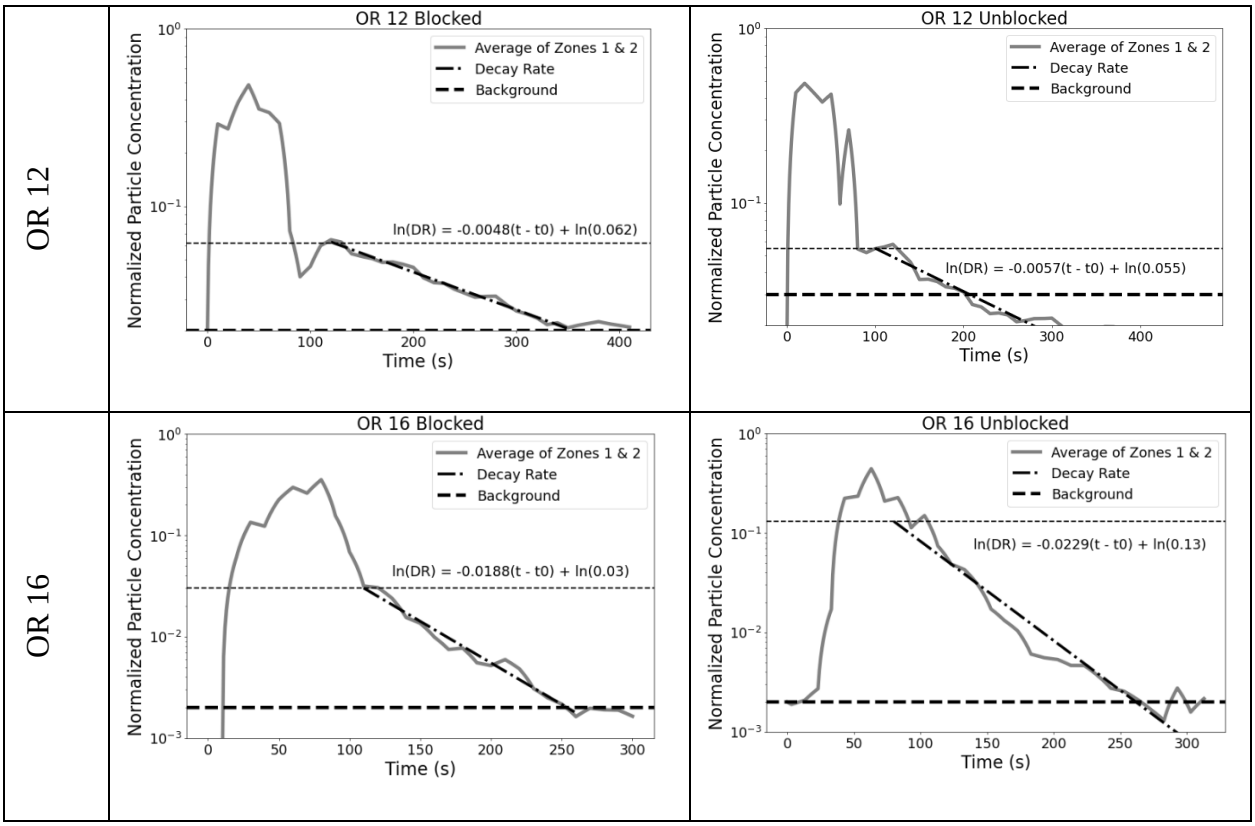

Supplementary Figure 1: OR indoor averages and decay rates